IEEE Access
Multidisciplinary | Rapid Review | Open Access Journal

Received 29 August 2024, accepted 27 October 2024, date of publication 12 November 2024, date of current version 9 December 2024.

Digital Object Identifier 10.1109/ACCESS.2024.3496786

RESEARCH ARTICLE

Artificial Intelligent Model to Enhance Thermal Conductivity of TiO_2-Al_2O_3/Water-Ethylene Glycol-Based Hybrid Nanofluid for Automotive Radiator

MD. MUNIRUL HASAN[1], MD. MUSTAFIZUR RAHMAN[2], (Member, IEEE), MD. ARAFATUR RAHMAN[3], (Senior Member, IEEE), SURAYA ABU BAKAR[1], MOHAMMAD SAIFUL ISLAM[4], AND TAREK KHALIFA[5]

[1]Faculty of Computing, Universiti Malaysia Pahang Al-Sultan Abdullah, Pekan 26600, Malaysia
[2]Faculty of Mechanical and Automotive Engineering Technology, Universiti Malaysia Pahang Al-Sultan Abdullah, Pekan, Pahang 26600, Malaysia
[3]School of Mathematics and Computer Science, University of Wolverhampton, WV1 1LY Wolverhampton, U.K.
[4]Department of Management and Information Technology, St. Francis College, Brooklyn, NY 11201, USA
[5]College of Engineering and Technology, American University of the Middle East, Egaila 54200, Kuwait

Corresponding authors: Md. Mustafizur Rahman (mustafizur@umpsa.edu.my) and Tarek Khalifa (tarek.khalifa@aum.edu.kw)

This work was supported by Universiti Malaysia Pahang Al-Sultan Abdullah under International Publication Research under Grant RDU223301.

ABSTRACT Vehicular cooling system is one of the priorities for the automobile industry, aiming to achieve sustainability and energy efficiency. Currently, coolants are being utilized in cooling systems that exhibit super heat transfer capabilities. Hybrid nanofluids as a coolant is offer enhanced heat transfer rate and improved efficiency and eco-friendliness of vehicle engine cooling systems. This study aims to analyze the conductivity of a hybrid nanofluid consisting of distilled water and ethylene glycol (in a ratio of 40 and 60) with Al_2O_3 and TiO_2 particles to evaluate its suitability as a coolant for vehicle engines using intelligent techniques. The volume concentration and the temperature varied from 0.02%-0.1% and 30 °C-80 °C, respectively. The experimental findings led us to develop an artificial neural network (ANN) model. This model consists of a layer containing 9 neurons designed to estimate thermal conductivity. ANN model was constructed using input parameters such as volume concentration and temperature, with the output being the conductivity. Furthermore, apart from utilizing the ANN, we employed techniques like support vector machine (SVM) and curve fitting (CF) approaches to analyze the experimental data. This allowed us to calculate values such as the correlation coefficient (R) and mean square error (MSE). The increase in thermal conductivity reached a maximum of 40.86% when the temperature was 80 °C, and the volume concentration was 0.1%. The results obtained indicate that the suggested ANN model aligns closely with the experimental data. Based on the assessment of the highest R-value and lowest MSE, this analysis demonstrates performance, with an R-value of 0.9998 and an MSE of 3.87415×10^{-06}. The training and testing phases exhibit remarkable performances with values of 4.86256×10^{-07} and 2.540599×10^{-06}, respectively. Moreover, when comparing the SVM and CF approaches, it was found that ANN modelling provided a level of accuracy in predicting the enhancement of conductivity in the hybrid nanofluid. These results demonstrate that the ANN can accurately predict thermal conductivity.

INDEX TERMS Thermal conductivity, hybrid nanofluids, artificial neural network, support vector machine, curve fitting.

I. INTRODUCTION

In the modern era, the surge in vehicle numbers on roads has highlighted significant challenges in energy sustainability

The associate editor coordinating the review of this manuscript and approving it for publication was Ye Zhou.

and environmental impact [1]. This growing number of automobiles substantially contributes to carbon dioxide emissions and other pollutants, exacerbating global warming and resource depletion. Consequently, automotive industries face stringent international regulations to reduce greenhouse gas emissions and improve energy efficiency [2]. One critical aspect of these efforts is enhancing engine cooling systems, which are vital for maintaining engine performance and reducing energy consumption. According to recent studies, cooling systems lose almost 30% of the energy from petroleum in car engines, emphasizing the need for more energy-efficient technology [3]. Therefore, reducing energy consumption and preserving the optimal temperature within the cooling system are pivotal factors in vehicle engine functionality. Despite the promising advancements in hybrid nanofluid research, the practical application of these fluids in automotive cooling systems still faces significant challenges [4]. These include the optimization of nanoparticle concentration and the control of fluid dynamics under operational conditions. Additionally, there is a gap in effectively predicting and enhancing the thermal conductivity of hybrid nanofluids explicitly tailored for automotive applications [5].

An investigation in the ANN model for predicting thermal conductivity enhancements of TiO_2-Al_2O_3/water-ethylene glycol-based hybrid nanofluid indicated excellent results for application in automotive and thermal management industries. With such excellent thermal conductivity characteristics, these ANN-optimized nanofluids are applied in radiators and have proven efficient in cooling function and maintaining the engine's optimum temperature, which works magnificently under extremely high-performance conditions. Such enhancement of the cooling capacities is vital to avert overheating and significantly increase the overall engine reliability. Using ANN-optimized nanofluids helps automotive designers develop compact and lightweight designs of radiating systems without losing cooling efficiency, resulting in better vehicle performance and improved handling characteristics. Especially when it comes to electric and hybrid vehicles, this innovation is vital due to the need for effective battery thermal management to ensure performance, safety, and durability. The optimized nanofluids exhibit better-cooling properties, enabling faster charging and overheating avoidance, which would be a convenience for the user and an addition to the battery life span. The efficiency improvements extend beyond direct cooling performance. The reduced demands on cooling system components of ANN-optimized nanofluids, including lower fan speeds and reduced coolant flow rates, minimize cooling system power consumption. This decrease in energy usage helps to provide a better fuel economy. In addition, the increased thermal management capabilities allow engines to operate more consistently and maintain optimal thermal management capabilities, resulting in better combustion efficiency and lower greenhouse gas emissions, which helps preserve environmental sustainability. Artificial intelligence (AI) models trained on nanofluid thermal performance data facilitate real-time monitoring and prediction of radiator cooling efficiency. With such predictive maintenance capability, potential problems can be identified, service could be planned, and radiator life could be extended, therefore keeping system downtimes to a minimum. The increased thermal management efficiency and predictive maintenance capabilities illustrate a richer automotive cooling technology with a perception, paradigm, and practice shift encompassing the multi-faceted areas of performance, efficiency, sustainability, and maintenance.

In this study, an ANN model was developed in order to mitigate the significant hurdles of thermal management system optimization and also raised thermophysical properties with a new kind of hybrid nanofluid (TiO_2-Al_2O_3/water-ethylene glycol) that is primarily suitable for automotive radiator applications. To do so, this investigation has a three-fold objective: (i) assessing how nanoparticle concentration and temperature influence the thermal conductivity of the nanofluid through experimental work; (ii) developing an ANN Model for predicting potential optimal thermal properties of the investigated nanofluid along with identifying relevant trends across such parameters as targets; and lastly (iii) investigating whether these artificial intelligence-based models are able to predict real-world data originating from ever more complicated designs effectively in comparison to traditional physics-based methodologies. The data obtained from these experiments will serve as inputs for the AI models. The ANN, SVM, and CF models will be trained with nanoparticle volume concentration, temperature, and thermal conductivity parameters. Model performance will be evaluated based on accuracy, precision, and the ability to generalize across different operational scenarios. The contributions of this research are itemized as follows:

∗ It advances the application of ANN in optimizing nanofluid formulations for automotive cooling systems, which has potential implications for improving vehicle energy efficiency and reducing environmental impact.

∗ The study provides a comparative analysis of ANN, SVM, and CF models in predicting the properties of hybrid nanofluids, contributing to the broader field of fluid dynamics and thermal engineering.

∗ It offers practical insights into the scalability of nanofluid production for industrial applications, considering both cost-effectiveness and environmental factors.

∗ The performance of the suggested models was examined and verified using correlation coefficient, mean square error, root mean square error (RMSE), and margin of deviation (MOD).

This study's ensuing sections are arranged as follows: Section II explores the previous related works; Section III describes the methods and materials; Section IV demonstrates the results and discussion; Section V performs a comparison among the models; and Section VI draws out the conclusion.

II. LITERATURE REVIEWS

A. HYBRID NANOFLUID IN VEHICLE ENGINE COOLING SYSTEM

Nanofluids show considerable potential as next-generation heat transfer fluids. Engineers have unlocked a new approach by suspending nanometer-scale particles in common bases like water (W), ethylene glycol (EG), and oil. These engineered colloids blend nanomaterials into typical working fluids, cultivating sophisticated and potentially more affordable solutions. While the dispersed solids are often merely 1 to 100 nanometers wide, their inclusion produces fluids with markedly amplified thermal properties. Going forward, diligent refinement of synthesis techniques and characterization of stability over time must be paired with insights into transport phenomena at the nanoscale to realize nanofluids' practical promise fully. Nanoparticles, when incorporated in fluids, have been shown to significantly improve the heat transfer properties of these fluids, which are higher than base fluid and even more effective than conventional thermic distributions [6]. This superior thermophysical behavior makes nanofluids a versatile medium applicable to broad industrial fields. The next evolutionary step in this domain is the formulation of hybrid nanofluids, which can be differentiated from their single-compositional identical by adding two or more different nanoparticles into a base fluid [7]. The multi-component strategy exploits synergistic effects among nanoparticles to improve thermal properties and performance. Including more nanoparticles in the base fluids has contributed to advancing heat exchange fluids in research, resulting in improved thermal conductivity properties [8]. As a result, hybrid nanofluids have the potential to significantly enhance the cooling efficiency of engines, thereby reducing the weight and simplifying thermal management systems [9]. Hybrid nanofluids can be classified based on the particles they contain. These categories include metal nanofluids (such as gold, silver, copper (Cu), and nickel), non-metal hybrid nanofluids (such as carbon nanotubes (CNTs) and graphene), and metal oxide hybrid nanofluids (such as zinc oxide, titanium dioxide, iron oxide, and aluminium oxide [10].

Nanofluids aim to improve the thermal conductivity of fluids, and nanofluid preparation is an indispensable process with two typical types: single-step techniques and a two-step homogenization method. The single-step synthesis method involves simultaneous nanoparticle generation and simultaneously dispersing them into the base fluid, whereas two-stepping separates these processes. The second has since found widespread use, especially in vehicle radiators, because of its low cost, scalability, and possible reduction in impurities. The advantages of this method include industrial facets in terms of large-scale production and comparatively fewer pollution sources that are reduced as long as the interphase is avoided during manufacturing; it provides more diversity since both nanoparticle type and base fluid can be chosen freely. These features contribute to the high portion of nanofluid production, especially in applied fields, e.g., automotive thermal management [11].

Jana et al. [12] were the first to introduce a combination of CNTs-Cu in nanofluids to assess its impact on thermal conductivity. Li et al. [10] investigated the use of ethylene-glycol-based silicon carbide (SiC)-multiwalled carbon nanotubes (MWCNTs) hybrid nanofluids as coolants in automobile engine cooling systems. They discovered that adding 0.4% volume of these nanofluids increased thermal conductivity by 32.01%. Their report found that the convective heat transfer coefficient of SiC-MWCNTs hybrid nanofluids was 26% higher than pure EG when tested under similar conditions. Jana et al. [12] carried out pioneering work in hybrid nanofluids. It was primarily that carbon nanotubes (CNTs) and copper (Cu) particles were combined to study their effect on thermal conductivity. Based on Li et al. [10], SiC-MWCNTs-based hybrid nano-coolants for automotive cooling systems have been investigated. Their research produced exciting results: a 0.4% volume of SiC-MWCNT hybrid nanofluid exhibited an impressive 32.01% increase in thermal conductivity compared to the base fluid. Hybrid nanofluids, as usual, provide an enhanced convective heat transfer coefficient compared with pure EG under similar experimental conditions, and when presented with the best results, it showed 26%. These findings confirm the synergy effects when employing more than one kind of nanoparticles (SiC and MWCNTs) and suggest hybrid nanofluids as promising in overcoming performance limitations related to single-component systems. Kumar and Sahoo [13] found that using a combination of spherical-Al_2O_3 and platelet-shaped graphene-nanoparticles in hybrid nanofluids resulted in performance as radiator coolants compared to using a combination of spherical-Al_2O_3 and cylindrical-shaped CNT-nanoparticles. The hybrid nanofluids with the combination exhibited an effectiveness of 2.94% while also showing an increase in entropy change in the air by 1.73% and in coolants by 1.62%. Nagarajan et al. [14] thoroughly examined the thermophysical properties of CuO and SiO_2 water hybrid nanofluids at various concentrations based on different temperatures. In their experimental work, a substantial heat transfer enhancement was obtained, where the maximum increase in heat transfer coefficient was 48.6% at a flow rate of 3 l/m and particle concentration of 0.2%. Kumar et al. [15] observed and studied the thermal performance of hybrid nanofluids fabricated with MWCNT and SiO_2. Their results showed significant cooling efficacy enhancements, with the temperature reduction reaching 40% and the total increase in air-cooling power. Asadi et al. [26] explored heat conduction in liquids containing multi-walled carbon nanotubes and aluminum oxide nanoparticles. Their investigation centered on how the amount of inclusions and degrees of temperature impacted thermal conductivity. Results demonstrated that boosting the quantity of the microscopic additives or raising the ambient warmth led the fluid to shuttle thermal energy more efficiently. More

significant frustrations of the blended nanomaterials or higher temperatures resulted in higher thermal conductivity readings. The findings signified discernible links between conductivity levels and the two variables examined. However, the research on the cooling substance still fails to meet the mentioned requirements. Hence, it is practically significant to explore hybrid nanofluids' properties and heat transfer capabilities in the context of vehicle radiators.

B. ANN APPLICATION

Recently, researchers have extensively utilized artificial intelligence (AI) technologies in various areas, including ANNs and SVMs, in nanotechnologies because of their flexibility and dependability in accurately optimizing the thermophysical properties of hybrid nanofluids [17], [18]. For example, using an ANN model, Alklaibi et al. [19] investigated the properties of Fe_3O_4–SiO_2/Water hybrid nanofluids. They used the Levenberg-Marquardt (LM) algorithm for training and tangent functions for activation with a 2-10-1 (two input neurons, ten hidden neurons, and one output neuron) network configuration. This architecture accurately represented the intricate relationships between nanofluid composition and properties. Rostam et al. [20], the thermal conductivity of hybrid nanofluid containing multi-walled carbon nanotubes (MWCNT), copper oxide (CuO), and water was predicted using the ANN model. Then, the performance of each model was calculated based on MSE values, and it showed a superior result that aligned well with experimental research. This methodology demonstrates the ability of artificial neurons to predict thermal properties with sufficient accuracy for an extensive, complex nanofluid system. Esfe et al. [21] used an ANN model to predict TiO_2-W nanofluid's thermal conductivity functionality. It was a 2-5-5-1 formation, including the LM training function and hyperbolic tangent sigmoid (tansig) activation functions. This particular arrangement was successful and capable of capturing the intrinsic non-linear relationship within nanofluid thermal conductivity. Rostamian et al. [22] performed ANN modeling experiments to evaluate hybrid nanofluids' thermal conductivity, incorporating CuO and single-walled carbon nanotubes (SWCNTs).

The outcomes of the computations revealed a direct correlation, wherein an escalation in particle concentration directly corresponded to an augmented thermal conductivity within the nanofluids. Pare and Ghosh [23] performed experimental analyses to examine the thermal conductivity of water-based nanofluids incorporating Al_2O_3, ZnO, and CuO. Additionally, they constructed an ANN model for the numerical estimation of these properties. The architecture of the model comprised a single hidden layer including 16 neurons. For training purposes, gradient descent was implemented as the training function, while tansig and purlin served as the activation functions in the hidden and output layers. Peng et al. [24] used a Multi-Layer Perceptron Artificial Neural Network (MLP-ANN) to predict the thermal conductivity of Cu-Al_2O_3 water/EG hybrid nanofluids. The simplified input to the proposed model was temperature and particle volume concentration, with a 2-10-1 architecture. The hidden and output layers used logarithmic sigmoid (logsig) activation functions, whereas the input layer had a purelin. The results showed good prediction accuracy and strong correlation with experimental values, indicating the potential of ANN models in predicting nanofluid properties. Hasan et al. [25] compared several activation functions to find the optimum ANN model for predicting thermal conductivity in EG/water-based cellulose nanocrystal (CNC) nanofluids. They found that the tansig was the best activation for this application. Asadi et al. [26] developed a genuinely applicable machine-learning technique in nanofluid research. The SVM algorithm was used to estimate the thermophysical properties of MWCNT-ZnO hybrid nanofluids in the volume fraction range of 25–75%. Efse et al. [27] utilized ANN and CF methods to predict the optimal MWCNT-ZnO/SAE 40 nano-lubricant parameters. The exceptional transit capacity, speed, efficiency, flexibility, enjoyable ride, low physical effort, and significant economic impact of vehicles have led to their immense appeal. Therefore, developing an efficient cooling system that consumes less energy and less carbon dioxide emissions is essential.

III. METHODS AND MATERIALS

A. PREPARATION OF HYBRID NANOFLUID AND STABILITY ANALYSIS

This study involves creating hybrid nanofluids through a two-step synthesis approach, as illustrated in Figure 1. To prepare the hybrid nanofluids, we have utilized two kinds of nanoparticles, including TiO_2 and Al_2O_3. Additionally, we have added a mixture of ethylene glycol and water (in a ratio of 60:40) as the base fluid. The properties and features of TiO_2 and Al_2O_3 nanoparticles, along with the base fluids, are presented in Table 1. The volume concentration of TiO_2-Al_2O_3 hybrid nanofluids was determined by applying Equation (1) where m_{np} and p_{np} denote the mass and density of the nanoparticles and m_{bf} and p_{bf} denote the mass and density of the base fluids. In this analysis, the ratio of TiO_2 and Al_2O_3 nanoparticles is 80:20. The selection of this ratio is based on its ability to create fluidity in a solution containing 40% EG. For an understanding, refer to the comprehensive explanation provided in the previous article [28]. According to the investigation, it was noted that among the tested ratios (20:80, 40:60, 50:50, 60:40, and 80:20) for TiO_2:Al_2O_3 nanoparticles, the 80:20 ratio exhibited the greatest stability concerning both zeta potential and absorption. Moreover, no indications of sedimentation were observed at this ratio. Subsequently, a blend of TiO_2 and Al_2O_3 was employed in the creation of hybrid nanofluids, using an 80:20 ratio. These nanofluids were generated at five different volume concentrations, specifically ranging from 0.02% to 0.1% with concentrations of 0.02, 0.04, 0.06, 0.08, and 0.1. A magnetic stirrer is employed for a duration of

TABLE 1. Properties of nanofluids containing titanium dioxide and aluminium oxide and base fluids such as water and EG.

Nanofluid							
	Colour	Ration	Melting point (^{0}C)	Boiling point (^{0}C)	Molecular mass (gmol^{-1})	Density (kgm^{-3})	Ref
Al2O3	White	13	99.8	101.96	4000	40	[29]
TiO2	White	5-6	>99	79.86	4230	8.4	
basefluid							
	Colour	Ration	Melting point (^{0}C)	Boiling point (^{0}C)	Molecular mass (gmol^{-1})	Density (kgm^{-3})	Ref
Water	Colourless and clear	60%	0.00	100	18.02	998.21	[30]
EG(C2H6O)	Colourless and clear	40%	-12.9	197.3	62.07	1113.20	[31]

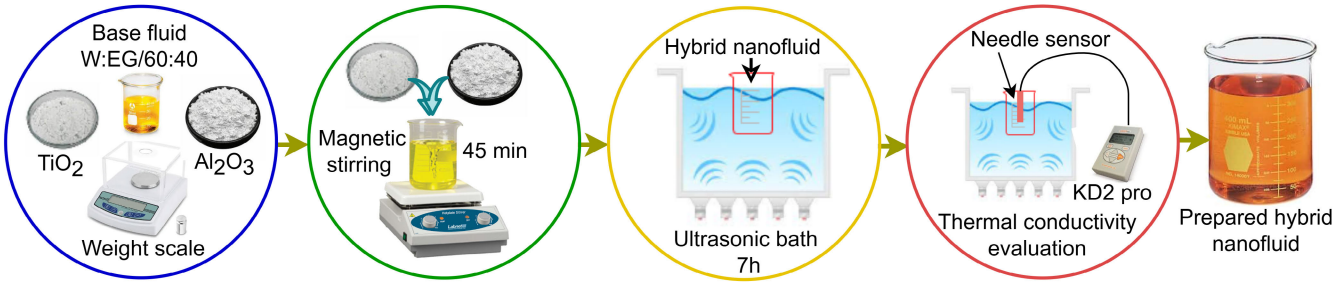

FIGURE 1. Hybrid nanofluid preparation.

45 minutes to mix the base fluid with the two measured nanoparticles.

$$\phi = \frac{(a_{np}/b_{np})}{(a_{np}/b_{np} + a_{pf}/b_{pf})} \times 100 \quad (1)$$

After that, the mixture is placed in an ultrasonic bath for seven hours to enhance its stability without using any surfactant. The sizing analysis of the TiO_2-Al_2O_3 hybrid nanofluid is conducted using the transmission electron microscopy (TEM) technique. Figure 2 illustrates the TEM visuals of singular TiO_2 nanoparticles, Al_2O_3 nanoparticles, and the amalgamation of TiO_2 and Al_2O_3 nanoparticles. The stability of hybrid nanofluids consisting of TiO_2 and Al_2O_3 is assessed using absorbency analysis conducted with a UV spectrophotometer (Genesys 50), zeta potential testing performed with a particle size analyser (Malvern Zetasizer Ultra DKSH) and visual observation. Several articles have employed these techniques to analyse stability. For instance researchers, in citations [32] and [33] employed the approach of visual sedimentation and UV–Vis spectrophotometry. Another way to analyse stability is, by estimating the zeta potential [34]. Numerous researchers have employed this test to provide insights into the evenness of colloidal suspensions uniformity [35], [36]. In this analysis, all three of these methods have been utilized for a period. Consequently, the findings of the stability study have become more accurate and reflective of reality.

The designed concentrations of TiO_2-Al_2O_2 nanoparticle nanoparticles in water-ethylene glycol base fluid used in the experimental investigation, which range from 0.02% to 0.1%, are chosen considering preliminary investigations showing remarkable thermal conductivity enhancement at even these low concentrations. The low concentrations have been selected for this study as they both facilitate more favourable thermal characteristics while minimizing the

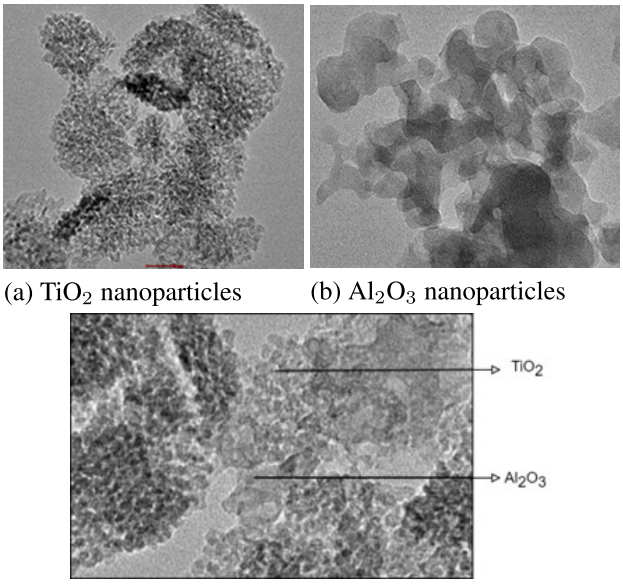

(a) TiO_2 nanoparticles (b) Al_2O_3 nanoparticles

(c) TiO_2-Al_2O_3 hybrid nanofluids

FIGURE 2. TEM images of single and hybrid nanofluids.

implications of aggregation and sedimentation phenomena often present at higher concentrations, potentially detracting from fluid stability and heat transfer performance. The experimental thermal characterization was performed across a temperature range of 30 °C to 80 °C in 5 °C increments corresponding to normal operating conditions for an automotive cooling system. This methodology sets thermal baseline characteristics at 30 °C (for standard operating conditions), measures performance over elevated temperatures to 80 °C simulating radiating peak thermodynamic states where increased conductivity dominance is essential for effective heat dispersion, and investigates

temperature-dependent interactions of nanoparticles with the base fluid, necessary to understand the mechanisms behind thermal transport. Despite the nature of nanoparticle characteristics such as complex shape and surface morphology, which is less influential in low concentration regimes because the nanoparticles act effectively as solute particles in solution, it can be said thermophysical properties could be manipulated while keeping a delicate balance between colloidal stability and thermal conductivity enhancement based on needs and transformation conditions. Such a temperature range supports comprehensive investigations of the role of temperature-dependent particle–fluid interactions and the effect of different thermal transport mechanisms on the overall thermal conductivity, heat transfer enhancement characteristics, and colloidal stability under variable-temperature conditions, thereby ensuring that reliable data can be taken for assessment of the performance of hybrid nanofluid over a broad spectrum of realistic operating conditions typical in many practical thermal management applications.

B. THERMAL CONDUCTIVITY MEASUREMENT

The thermal conductivity of TiO_2-Al_2O_3 hybrid nanofluids is carefully measured using the advanced KD2 Pro thermal property analyzer (Decagon Devices, Inc.). Sample regulation occurs using a high-precision water bath to enable temperature control. Following ASTM D5334 and IEEE 442-1981 standards, the KD2 Pro sensor is positioned vertically within a sample to (i) maximize data fidelity while minimizing measurement artifacts [37]. The experimental matrix covers a wide range of temperatures (30–80 °C), measured in 5°C steps, generating an extensive dataset including eleven different thermal points. To enhance measurement reliability while mitigating transient fluctuations, a multi-step approach was instituted: for each unique pairing of temperature and volume concentrations, ten independent trials were performed consecutively, allowing 10-15 minutes between successive experiments to ensure thermal equilibrium was established. The definitive thermal conductivity for each experimental condition was then derived as the arithmetic mean of these repetitive measurements. This methodology guarantees high-fidelity reproducible data and provides a robust foundation for the in-depth profiling of thermal transport attributes in TiO_2-Al_2O_3 hybrid nanofluids across various operational parameters. This consequently facilitates more accurate predictive modeling and optimized use within progressive thermal management architectures. Meanwhile, a brief trial was occasionally conducted to assess stability over prolonged periods. On other occasions, alternative measurement devices were employed to validate consistency. Overall, this exhaustive exploration lays the groundwork for advances in thermal engineering solutions.

C. VALIDATION OF EXPERIMENTAL DATA MEASUREMENT $R_A = A/A_O$

The LVDV III Ultra Rheometer and KD2 Pro reliability validation involves comparing the current thermal conductivity values for 40% EG with the ASHRAE data [38] within the 30–80 °C temperature range with an interval of 5 °C. Various researchers have employed this validation approach. The maximum deviations observed were 2.5% and 1.6% compared to the tests conducted by Vicki, Abdullah, Gunnasegaran [39], and Reddy and Rao [40], respectively. The validity of thermal conductivity measurements, as depicted in Figure 3, exhibits a maximum deviation of 0.5. Consequently, it can be affirmed that these devices are reliable and productive for measurement purposes with minimum variation. Additionally, in the context of thermal conductivity, the features of 40% EG demonstrate a pattern of both increase and decrease with temperature fluctuations.

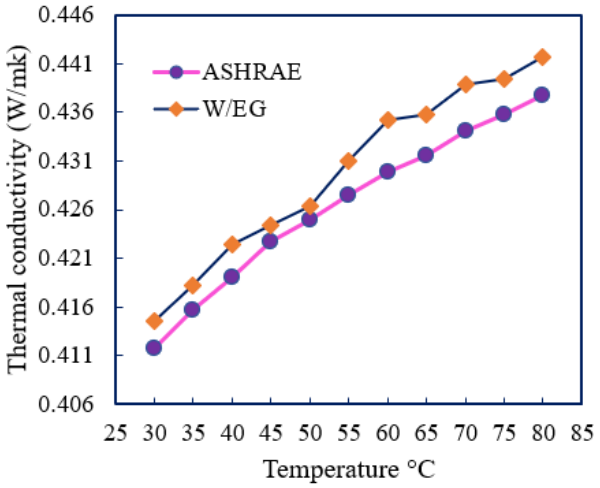

FIGURE 3. Validation measurement of thermal conductivity with LVDV III Ultra Rheometer and KD2 pro analyzer.

D. INTELLIGENT ARTIFICIAL NEURAL NETWORK

Artificial neural networks are the most potent and widely accepted computing systems, and the human brain's biological neurons inspire them. ANN is a branch of machine learning and a foundation of deep learning models. Nowadays, it provides a dynamic way to simulate complicated and obscure problems in all sections of science and engineering. The ANNs comprise layers of neurons that serve as the network's processor. The input and output layers, located at the network's two ends, receive input data and features accordingly and predict the expected result in the output layer. Between the input and output layers, one or more hidden layers are in charge of most network calculations [41].

To narrate the overall performance of an ANN, each feature is assigned as an input to each of the neurons in the input layer, and this input data is passed to the output layer through the connection within these layers, the way every neuron in the preceding layer, with weights connects to the subsequent layer neurons. In other meaning, a bias value is associated with each neuron in the prior layer, which will be attached to the obtained values by multiplying the neurons of the preceding layer with the weights. After that,

this value will transfer to the activation function, and the value of the next layer neuron will be determined. Similarly, the communication between the input and output will be established by hidden layers. The values of the biases and weights must be updated to train the network so that the prediction value of the network gets close to the actual output value, which usually reduces the number of errors mentioned in the prediction of the network. The derivative chain method can be employed to update the learning parameters of the network about the considered parameters, which move to the input layers from the output layers. This backward-and-forward process continues as far as the optimal parameters for the network are achieved and the training period is completed [42]. An ANN neuron can be mathematically represented as a basic model in which the input value (p_i) is multiplied by the i_{th} weighting factor of the k^{th} neuron. This value is summed up by the bias (b_k), and σ is the activation function. Then, an ANN neuron can be expressed mathematically, as in Eq. 2.

$$y_k = \sigma\left(\sum_{i=1}^{n} w_{ki}p_i + b_k\right) \tag{2}$$

The primary goal of the ANN in this study is to adjust the composition of the TiO_2-Al_2O_2/water-EG hybrid nanofluid to improve its thermal conductivity. The model employs ANN to forecast the effects of different concentrations and temperature ranges on thermal conductivity, facilitating the precise adjustment of nanofluid parameters. This allows engineers to attain superior cooling efficiency in automobile radiators, facilitating enhanced thermal management, diminished overheating hazards, and increased reliability in high-performance applications.

E. ANN MODEL DEVELOPMENT

In this research, an ANN model is developed using MATLAB software (version 2020a). The temperature and volume concentration of nanofluid are in the input layer, and thermal conductivity is in the output layer. The developed ANN model has one hidden layer and one output layer where "Tansig" and "Purelin" are used as activation functions. Then, Eq (2) establishes mapping relations that can be written as follows:

$$y_k = purelin\left(\sum_{i=1}^{n} w_{ki}p_i + b_2\right) \tag{3}$$

where,

$$y_k = tansig\left(\sum_{i=1}^{n} w_{ki}p_i + b_1\right) \tag{4}$$

where, p_i and y_k input and output vectors, w_{ki} and w_{ij} are matrics of weight, b_1 and b_2 are biases of the hidden layer and output layer, respectively. Considering the problem complexity, data set, error goal, and the number of weights and biases, this study selects LM as a training algorithm that automatically sets appropriate values for the parameters of the objective function. The LM algorithm can improve the neural network's ability, solve the non-linear least square problems, and train the objective function. The sigmoid hidden layer and linear output layer enable the error propagation network architecture to estimate any function with limited points of discontinuity. Figure 4 illustrates the developed schematic network diagram.

The configuration of an ANN network, particularly the number of neurons in the hidden layer, significantly influences prediction accuracy and the network's generalization capability. Consequently, it is crucial to optimize this topology. However, no universal rule exists for establishing the optimal configuration of an ANN network; typically, it is determined through a trial-and-error approach [43]. In this study, the number of neurons was changed between 1 and 22, and the accuracy of the developed predicted ANN model is evaluated using various performance metrics including MSE, RMSE, R, and MOD defined in section F(4).

Algorithm 1 ANN Configuration Development

```
Begin
Input: Temperature and volume concentration;
Output: Thermal conductivity;
Build an ANN model;
Input, 1 hidden layer, and 1 output layer;
Initialize the training parameters;
for Each training epoch do
    perform standard training procedures;
    perform weight and biases updates;
    perform AF and TF updates;
    perform learning rate updates;
    for Each hidden layer do
        for Each neuron n of the hidden layer do
            Eliminate a portion of smallest weights;
            Eliminate a portion of smallest biases;
            Increase the number of neurons
            if n is the not least neuron numbers then
                Add more neurons until the best output;
            end if
            Find the suitable neuron numbers;
        end for
        Find the suitable hidden layers;
    end for
end for
Select the optimum network architecture;
Evaluate and test the ANN model;
```

The initial step in the ANN training process is making patterns the network can use to learn. ANN model development is described in algorithm 1. In this model, 55 input samples have been used in terms of the physics of the problem and divided into three categories: 70% of the data for training, 15% for testing, and 15% for validation. The split samples then enter the pattern network. Formally, define a hidden layer in an ANN and perform the training

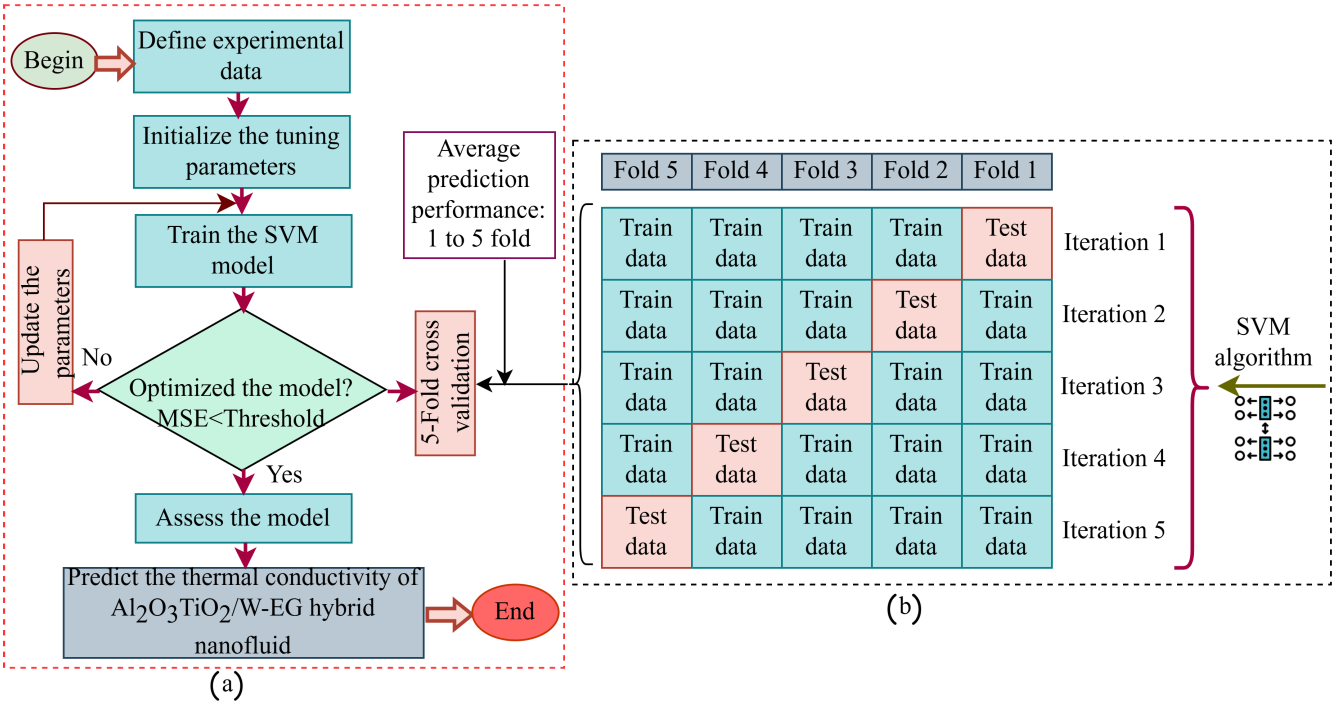

FIGURE 4. (a) Flowchart of SVM (b) The 5-fold cross-validation in SVM.

parameters. This layer comprises n^p neurons collected from a vector $v^p = [v_1^p, v_2^p, v_3^p \ldots . v_n^p]$. Any neuron within v^p is linked to a variable number of neurons in the below layer, v^{p-1}. For fully connected layers, the number of connections follows a quadratic relationship, i.e., $n^p n^{p-1}$. Nevertheless, this randomly created topology might not be well-suited to the specific data characteristics the ANN model attempts to learn. To address this issue, in the training process, following each training epoch, a portion of the smallest positive weights and the largest negative weights of the connections are eliminated. These excluded weights are those near zero, and it is anticipated that removing these less significant weights will not significantly impact the model's performance. Next, find the suitable number of neurons for hidden layers to develop an optimal topology.

F. SUPPORT VECTOR MACHINE

Support Vector Machine (SVM) is one of the most practical approaches to supervised machine learning, and it analyses the data for regression and classification issues. Vapnik initially proposed the SVM [44] for regression problems. Since then, it has been applied to a wide variety of tasks, including engineering science [45], biomedicine [46], social science [47], and many more. The SVR technique visually represents the non-linear relationship between input and output variables.

In addition to this, it demonstrates excellent characteristics such as a high repeatability and improved ability to generalize, particularly with a smaller number of datasets. By minimizing structural risk in favor of empirical risk, the SVR method can also address the overfitting issue and the lack of generalization in ANN models. In addition to this, it can predict the regression by using kernel functions defined within a high-dimensional feature space [48]. The SVR model's flowchart is presented in Figure 4(a).

In the given dataset P = p_1, p_2, $p_3 \ldots . . p_n$ and Q = q_1, q_2, $q_3 \ldots . . . q_n$ where p_n and Q_n denote the inputs and target variables, respectively. The objective of using SVR is to create a regression function f(p) that can forecast the target values q_1, q_2, $q_3 \ldots . . . q_n$ based on various inputs p_1, p_2, $p_3 \ldots . . p_n$. The regression can be mathematically expressed as follows [48];

$$q = \int (p) = w.\varphi(p) + b \tag{5}$$

where w, φ(p), and b indicate the weight vector, nonlinear mapping function, and bias, respectively. The primary input data are moved to a greater dimensions space using the mapping function φ, and the nonlinear separable problem is transformed into a linear separable problem in the same new space. The w and b are determined by minimizing the regularized risk function, as demonstrated below [49];

$$R_{rr}(C) = C\frac{1}{n}\sum_{i=1}^{n} L_\varepsilon \int (p), q + \frac{1}{2}w^2 \tag{6}$$

where $R_{rr}(C)$ and 1/2 w^2 denote the risk function and regularization factor. The C is a positive-valued coefficient, also known as box constraint, which controls the balance between the empirical risk and regularization factor. In this case, if C is a higher value, error minimization has been

prioritized more, which causes the tube to enlarge. Hence, the tube is a space that creates the margin of epsilon error. Conversely, a lower value of C indicates a more significant concern about higher tube minimization, which leads to an increase in inaccuracy [50]. $L_\varepsilon \int(p), q$ is the ε-insensitive loss function that is stated in Equation (7);

$$L_\varepsilon \int(p), q = \begin{cases} |\int(p) - q| - \varepsilon & for |\int(p) - q| \geq \varepsilon \\ 0 & otherwise \end{cases} \tag{7}$$

where ε refers to the epsilon error (ε), considered zero. The objective of applying the ε-insensitive loss function is to find a function f(p) that matches the training data with a deviation lower than or equivalent to ε [51]. This function must be as flat as feasible. Small w is necessary due to the function's flatness. Thus, Eq. (8) can solve the mentioned minimization problem.

$$Min_{w,b}\ \frac{1}{2}||w||^2$$
$$Subject\ to \begin{cases} q_i - w\varphi(p) - b \leq \varepsilon \\ (wp_i), +b - q_i \leq \varepsilon \end{cases} \tag{8}$$

where (p_i,q_i) refers to the training dataset and supposes that all training data sets are precisely approximated ε. Nevertheless, some variance exists to settle these. Eq. (8) can be rewritten by introducing slack variables ξ_i and ξ_i° as described in Eq.(9) [52];

$$Min_{w,b}\ \frac{1}{2}||w||^2 + C\sum_{i=1}^{n}(\xi_i - \xi_i^\circ)$$
$$Subject\ to \begin{cases} q_i - w, p_i - b \leq \varepsilon + \xi_i \\ (wp_i), +b - q_i \leq \varepsilon + \xi_i^\circ \\ \xi_i, \xi_i^\circ \geq 0\ i = 1, 2 \ldots . n \end{cases} \tag{9}$$

The slack parameters xi_i° and xi_i indicate the upper and lower bound of the excess deviation.

The objective function f(p) can be formulated as follows [52]:

$$\int(p) = \sum_{i=1}^{n}(\alpha_i^\circ - \alpha_i)k(p_i, p_j) + b \tag{10}$$

where k(p_i, p_j) is the kernel parameter responsible for mapping non-linear functions into a higher-dimensional space. Notably, SVR models use kernel functions to deal with the featured space's high dimensionality and computational complexity. One of three possible values exists: positive, symmetric, and semi-definite. Several models for kernel functions have been suggested in the literature, with the linear, sigmoid, polynomial, and radial basis functions being the most common. It can be either positive, symmetric, or semi-definite. Some examples of familiar kernel functions are as follows:

$$\Delta\ Linear - k(p_i, p_j) = (p_i, p_j) \tag{11}$$
$$\Delta\ Ploynomial - k(p_i, p_j) = (p_i, p_j + 1)^d \tag{12}$$
$$\Delta\ RBF - k(p_i, p_j) = exp(\frac{||p_i + p_j||^2}{2^2}) \tag{13}$$

where d is the degree of the polynomial. The polynomial kernel function is employed in this study. Several articles discuss SVM's elaborate concepts and procedures [53], [54].

TABLE 2. The optimal values for the SVM model's parameters.

Parameters	Values
Epsilon	0.0048
Box constraint	0.0483
Bias	0.5165
Kernal function	Polynomial
Kernal scale	1.2950
Kernal order	2
K folds	5
Number of iterations	32

1) SVM MODEL DEVELOPMENT

The thermal conductivity of nanoparticles is predicted using the SVR model, which is developed using temperature and volume concentration inputs. Similar to the ANN model, the MATLAB environment was used in the SVM model. The data set from the experiment was divided into two segments with a ratio of 70:30 for train and testing the model, respectively. The training dataset was employed for the development of the SVR model, whereas the testing dataset was utilized to assess and validate the performance of this model.

2) TUNING PARAMETERS SELECTION

Finding the optimal values for the SVR model's parameters is the only way to ensure high prediction accuracy and generalizability. The tuning parameters of the SVM model include kernel function (k), box constraint (C), epsilon (ε), and gamma (γ). The use of the optimization method to select the tuning parameters of the SVM model has a high tendency due to the constraints and shortcomings of the manual search method [55]. Therefore, the Bayesian method [56] was employed in this paper to find optimal parameters and suitable SVM formation. This way, a polynomial was selected as the kernel function for this analysis. The bias term, b, is included in the kernel, and the kernel function accommodates it. In a high-dimensional space, the epsilon represents the difference in value between the predicted and actual values. The box constraint is a parameter that assigns a penalty to vectors outside the epsilon-margin. The strength of the support vectors can be adjusted by changing the values of the box constraints. Since more data points are contained within the margin, the possibility of overfitting is diminished when the box constraint value is optimized. Support vectors can be identified by the points that fall within the margin. Table 2 displays the optimal values for the SVR models.

3) K-FOLD CROSS-VALIDATION

To prevent the overfitting problem, SVM algorithms frequently use cross-validation, which involves randomly splitting the database into N folds. Because of this, the SVM model is trained on N-1 folds and then evaluated on the Nth fold. This study, 5-fold cross-validation is used to divide the assembled dataset into the five different datasets shown in Figure 4(b). This process is repeated five times so that each fold in the dataset has an equal chance of being chosen as the validation dataset. In addition, a grid search modification is introduced to adjust the hyperparameters of training SVM models. The optimization is conducted by applying each feasible combination of parameters for a specific SVM algorithm.

4) PERFORMANCE EVALUATION

Performance metrics such as MSE, RMSE, MOD, and R were used in this research to evaluate the effectiveness of the ANN, SVM, and CF models. Equations (14), (15), (16), and (17) represent the expression of computing the MSE, R, RMSE, and MOD [27], [57]. Where m, V_exp, and V_pre represent the number of data samples experimental and predicted outcomes by the applied models. The differences between these two values should be minimized to achieve excellent performance.

$$MSE = \sum \frac{1}{m} \sum_{j=1}^{m} (V_{exp} - V_{pre})^2 \tag{14}$$

The R is employed to compare the outputs with the targets and indicates the strength of the relationship between the targets and outputs. The range of the R is between -1 and 1. When the value of R is positive 1, there is a solid interrelation among the data. On the contrary, negative 1 indicates a solid negative interrelation, and 0 means no connection between these two variables.

$$R = \frac{\sum[(V_{exp} - \lambda_{exp}) * (V_{pre} - \lambda_{pre})]}{\lambda_{exp} * \lambda_{pre}} \tag{15}$$

where, λ_{exp} and λ_{pre} are the mean values of V_{exp} and V_{pre} similarly λ_{exp} and λ_{pre} are considered standard deviations of V_{exp} and V_{pre},, respectively. The results indicated in Table 5 show that the lowest values of MSE and higher values of R are considered optimum outcomes, and these were obtained with nine neurons in the hidden layer. The RMSE and MOD values are calculated from the equations below. Like MSE, the lowest values of RMSE and MOD are also considered optimum results.

$$RMSE = \sum \sqrt{\sum \frac{1}{m} \sum_{j=1}^{m} (V_{exp} - V_{pre})^2} \tag{16}$$

$$MOD = |\frac{V_{exp} - V_{pre}}{V_{exp}}| * 100 \tag{17}$$

G. CURVE FITTING METHOD

Curve fitting is a robust and widely used technique for determining the "best fit" model of the connection between independent and dependent variables [58], [59]. This technique is based on QR factorization and was created and coded by D'Errico [60]. Several forms of curves are used in a variety of mathematical contexts. The most popular types of curve models are detailed in Table 3. The regression equation for each curve version is solved, and the resulting values are compared to the actual values to determine the best-fit [61]. Thermal conductivity is the dependent variable on this issue, while temperature and volume concentration are the independent variables. This comparison contributes to calculating the error value for each curve described earlier.

TABLE 3. Different curve with general equation.

Curve model	Curve equation
Straight line (polynomial)	z=p_1.x+p_2
Cubic curve (polynomial)	z=p_1.x^3+p_2.x^2+p_3.x+p_4
Parabolic curve (polynomial)	z=p_1.x^2+p_2.x+p_3
Polynomial (n)	z=p_1.x^n+p_2.x^{n-1}+....+p_n
Exponential curve	z=a.e^{bx}
Geometric curve	z=a.x^b+c

IV. RESULTS AND DISCUSSION

A. STABILITY ANALYSIS

1) MEASUREMENT OF ZETA POTENTIAL

The measurement of zeta potential is a fundamental quantitative approach for assessing nanofluid stability based on the electrophoretic behavior of nanofluids [62]. The primary advantage is the simplicity and speed of the test. Increased zeta values correspond to higher nanoparticle repulsive forces, enhancing stability. Based on the articles [36] and [63] the zeta potential value is >30mV, indicating good stability. Table 4 provides the standard range of zeta potential values, a vital indicator in colloidal science. In this study, the zeta potential measurements are employed to measure the dispersibility of nanoparticles into base fluid. The experimental setup consists of an initial examination done immediately after preparation of the nanofluid, as well as a repeat assessment following 15 days. The peak absolute value of Zeta potential is 43 mV for freshly prepared TiO_2-Al_2O_3/W-EG hybrid nanofluids, indicating excellent colloidal stability.

TABLE 4. Stability level and zeta potential [31].

Stability	Zeta potential (±mv)
Little or no stability	0
Some stability	15
Moderate stability	30
Good stability	45
Finest	60

Figure 5 elucidates the zeta potential values across a spectrum of nanofluid concentrations. In colloidal science,

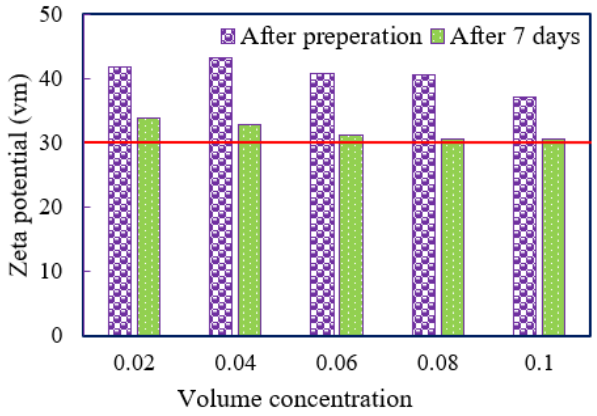

FIGURE 5. Values of zeta potential at different volume concentrations.

a zeta potential magnitude of 30 mV is widely recognized as the threshold for good stability. Notably, this study reports a minimum zeta potential of 37.1 mV, significantly exceeding this benchmark. This elevated value indicates superior electrostatic stabilization and suggests exceptional nanofluid stability. Furthermore, the persistence of favorable zeta stability across all nanofluid samples, even after 15 days, underscores the robust nature of the colloidal dispersion. This temporal stability is particularly noteworthy, implying resistance to agglomeration and sedimentation processes that often plague nanofluid systems. The consistently high zeta potential values observed across varying concentrations and time points validate the preparation method's efficacy and suggest promising long-term stability characteristics. These findings have significant implications for the practical application of these nanofluids in various thermal management and heat transfer scenarios.

2) VISUAL OBSERVATION

The stability of the tested nanofluids is evaluated through periodic sedimentation photography over one month. This methodology for characterizing suspension stability has been corroborated by other researchers in the field [33], [64]. Figure 6 presents a time series of sedimentation photographs for TiO_2-Al_2O_3 nanofluids. The photographic evidence demonstrates that all samples maintain excellent stability for two weeks. In the third week, some nanoparticles exhibit sedimentation, a phenomenon potentially attributable to gravitational forces and enhanced van der Waals interactions between particles [56]. Complementing the visual analysis, spectral analysis using UV-Vis spectroscopy confirms the stability of TiO_2-Al_2O_3/W-EG hybrid nanofluids over two weeks.

This dual approach to stability assessment provides a comprehensive evaluation of the nanofluid's temporal behavior. The present study achieves suspension homogeneity solely through a 7-hour ultrasonication process. However, future investigations may explore alternative strategies to enhance long-term stability. These potential avenues include

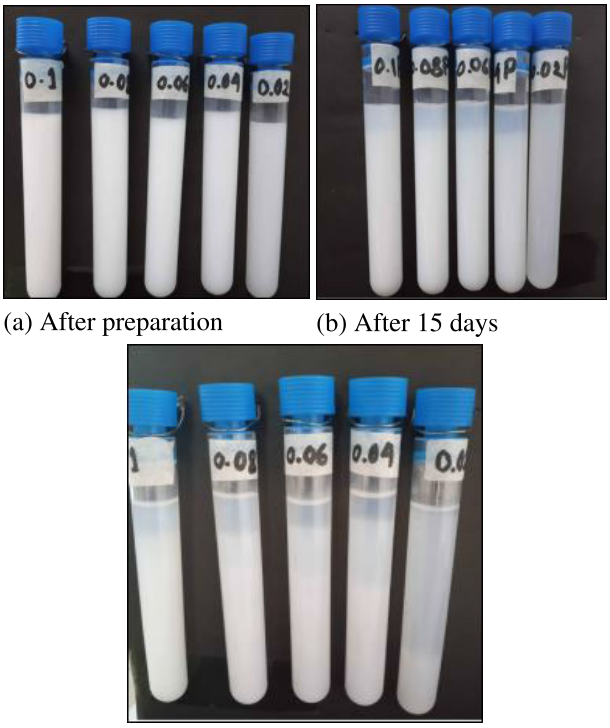

(a) After preparation (b) After 15 days

(c) After 30 days

FIGURE 6. Sedimentation condition of TiO_2-Al_2O_3/W-EG hybrid nanofluids.

the incorporation of surfactants and the modification of nanoparticle surfaces. Such approaches could significantly contribute to developing more stable nanofluid formulations, thereby expanding the scope and applicability of these colloidal systems.

3) UV–VIS SPECTRAL ANALYSIS

The stability of the nanofluids is measured quantitatively by UV-Vis spectral analysis using a Genesys 50 UV-visible spectrophotometer. This analytical method uses the wavelength characteristic of a sample by spectroscopic technique. The spectral profile of 903 nm is where peak absorption occurs for each sample. Nanofluid absorption is evaluated based on light intensity measurement by comparing nanofluid samples for base fluid [66]. The comparative nature of this method allowed for exact quantification of the increase in optical properties of suspension due to contribution either directly or indirectly by way of nanoparticle effect - thus providing an idea about stability and uniform distribution system.

The absorbance ratio and sedimentation time variations under specific ultrasound durations The absorbance ratio with sedimentation time for different ultrasonication times is shown in Figure 7. Eq. (18) is used for the absorbance ratio measure of a sample.

$$R_a = \frac{A}{A_\circ} \tag{18}$$

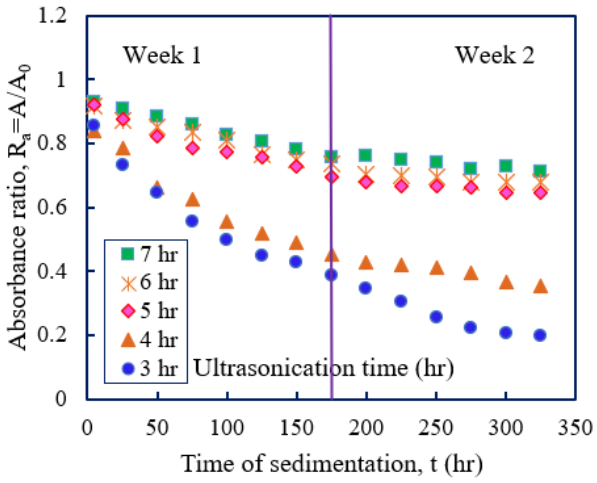

FIGURE 7. The absorbance ratio and sedimentation time variations under specific ultrasound durations.

where R_a indicates the absorbance ratio, A is the final absorbance at a particular time, and $A_\circ$ is the elementary absorbance of the sample. The absorbance ratio of 1 is considered a sign of great stability in suspension. This approach to an analytical stability assessment has been widely supported and confirmed by other researchers [67], [68], so this review treats the input as a scientifically reliable form of necessity for stability testing already on that level. The plot of absorbance ratios, which shows the comparative degradation versus different ultrasonication times, is displayed in Figure 7. Interestingly, samples sonicated for 7 hours show the highest absorbance ratio, remaining over 70% after a week. This outperforms the performance of samples prepared with shorter ultrasonication times (3, 4, 5, and 6 hours). These results strongly support that the nanofluid used in this paper is best realized after sonication for 7 hours. A detailed protocol that produces samples with solids suspension characteristics extending for over two weeks is described here. This is important to ensure the stable performance and reliability of the nanofluid over a longer period while it finds its way into more applications.

B. THERMAL CONDUCTIVITY OF TIO_2-AL_2O_3

Figure 8(a-b) shows the thermal conductivity evaluation results of TiO_2-Al_2O_3 hybrid nanofluids at volume concentrations (0.02% to 0.1%) and temperatures between 30 −80 °C, which indicates that their elevated values reveal a significant increase in comparison with ASHRAE [38] typical value for thermal conduction reacting over standard EG level due to nano-particles existent onboard as it comprises distinguished characteristics than surrounding fluid molecules. The nanoparticle volume concentration and temperature positively affect the thermal conductivity. The increase in thermal conductivity with the increasing nanoparticle concentration is called the extension of the nanoparticle surface [69]. At the same time, improving Brownian motion intensifies particle collisions and causes a temperature-dependent increase in thermal conductivity [35]. This particle interaction is enhanced, which results in increased kinetic energy transfer, leading to higher thermal conductivity. In order to visualize these multivariable relationships comprehensively, contour mappings of thermal conductivity vs temperature and volume concentration are plotted in Figure 8(c). This map identifies the areas of highest thermal conductivity, corresponding to higher temperatures and volume fractions. The analysis of how thermal conductivity enhancement is performed quantitatively by Equation (19). The significant enhancement up to 40.86% at 80°C shows that, once again, higher Al_2O_3 loading (0.1%) can be applicable for high-temperature applications with substantial improvement in heat transfer coefficient and effectiveness of these hybrid nanofluids. Figure 8(d) provides a side-by-side visual comparison of increases in thermal conductivity within the experimental matrix ((w/c, T). This visualization made locating the optimal formulation parameters easier according to requirements. The measured thermal conductivity enhancements in TiO_2-Al_2O_3 hybrid nanofluids show the combined effect of temperature and nanoparticle volume concentrations. Those results indicate a crucial role of nanofluids at the most fundamental levels for designing and optimizing novel heat transfer fluids and as noteworthy consequences in multiple industrial applications.

Increment of thermal conductivity(%) =

$$(\frac{K_{nf}}{K_{bf}} - 1) * 100 \tag{19}$$

C. THERMAL CONDUCTIVITY COMPARISON WITH AL_2O_3 AND TIO_2

Comparison of the thermal conductivity results of TiO_2-Al_2O_3/W-EG hybrid nanofluids with their single-component counterparts, Al_2O_3 and TiO_2. Here proceeds the synthesis of single-component TiO_2 and Al_2O_3 nanofluids dispersed in 40% EG base fluid at a volume concentration of 0.1%, respectively, via a two-step method for this need. These single-component nanofluids have been tested for thermal conductivity measurements at 30 °C, 50 °C and 70°C. The thermal conductivity profiles of the hybrid and individual nano-fluids are shown in Figure 9. TiO_2-Al_2O_3 hybrid nanofluid also presents better thermal conductivity than both TiO_2 and Al_2O_3 single-component nanofluids in the temperature range that we investigated, as shown.

It is worth mentioning that the TiO_2 nanofluids are of lower thermal conductivity compared to other samples tested, and for all these hybrid counterparts, it can be seen that those based on the TiO_2-Al_2O_3 mixture show higher conductivities. The superior enhancement in thermal conductivity can be attributed to a synergistic effect leveraging the combination of single-phase and biphasic nanoparticles. The interaction between TiO_2 and Al_2O_3 nanoparticles seems to make a more effective thermal transport network in fluid, resulting from this improvement and higher enhancement of its overall thermophysical properties. The advantages of the hybrid

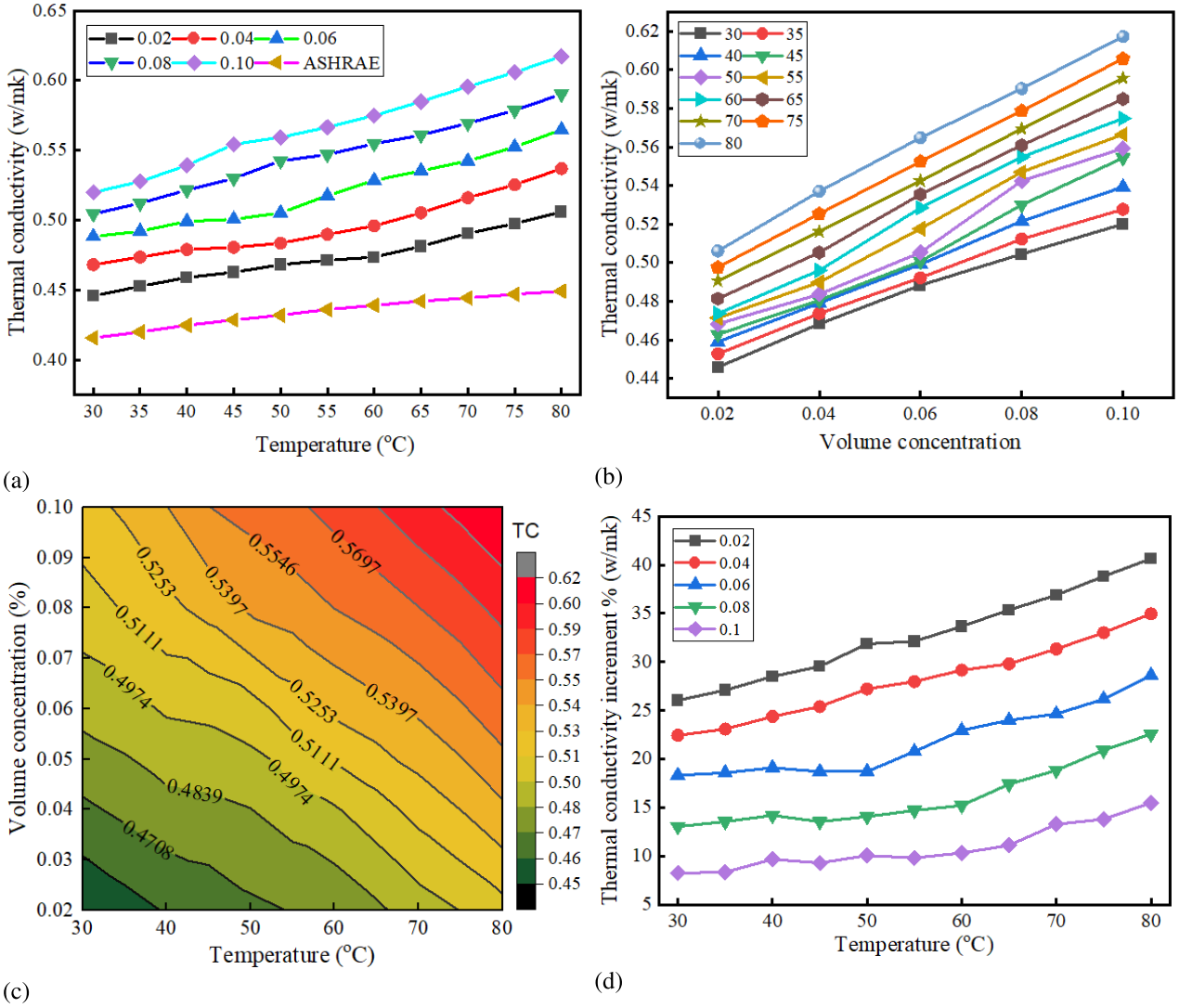

FIGURE 8. (a) Variation of thermal conductivity with temperatures (b) Variation of thermal conductivity with volume concentrations (b) 3D contour plot of thermal conductivity against temperatures and volume concentrations (d) Thermal conductivity enhancement against temperatures.

nanofluid regarding practical heat transfer application lie in its hugely improved thermal conductivity. The enhanced thermal properties could result in improved heat exchange systems with lower energy usage and better performance across different thermal management applications.

D. PREDICTION OF HEAT TRANSFER EFFICIENCY

The properties enhancement ratio (PER) is one of the most influential parameters for evaluating heat transfer performance in 40% EG-based TiO_2-Al_2O_3 hybrid nanofluids. This non-dimensional parameter, the ratio of thermal conductivity enhancement to viscosity enhancement gives vital information about what governs fluid performance in internal laminar flow regimes [70], [71]. If a PER value is less than five (PER < 5), this means that the heat transfer efficiency of nanofluid compared with classical fluids will be better, and so it can serve as a quantifiable criterion for performance assessment [70].

Figure 10 presents profound insights into the interplay between temperature, concentration, and enhanced thermal performance for TiO_2-Al_2O_3 hybrid nanofluids. Data across the comprehensive experimental design reveal two distinct behavioral patterns. At concentrations of 0.06%, 0.08%, and 0.1%, PER values consistently remained below the critical five-unit threshold, signifying superb heat transfer potential for demanding applications. In contrast, 0.02% and 0.04% volume concentrations exhibited more significant variability in PER readings that occasionally surpassed five units. This suggests a narrower range of effectiveness for heat transfer tasks, restricting versatility. Overall, optimal hybrid nanofluid formulation requires a judicious selection of concentration levels to ensure robustly lowered PER indications across diverse operational conditions. The reason for such bifurcation in the performance can be seen as a non-linear relationship between nanoparticle concentration and thermal property enhancement. The addition of nanoparticles to

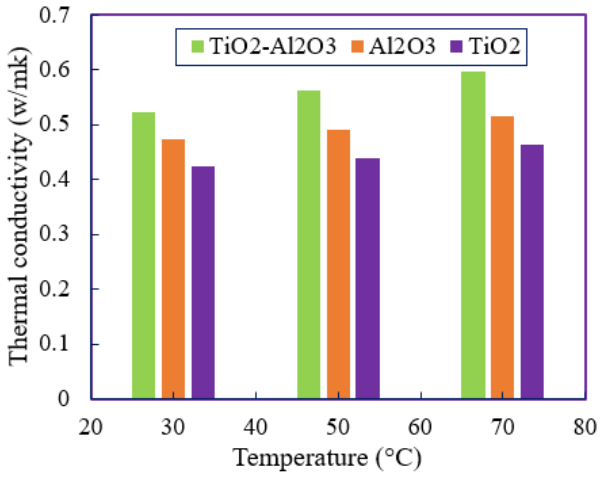

FIGURE 9. Comparison of the thermal conductivity of single (TiO_2 and Al_2O_3) and hybrid nanofluids (TiO_2-Al_2O_3) with a volume concentration of 0.1%.

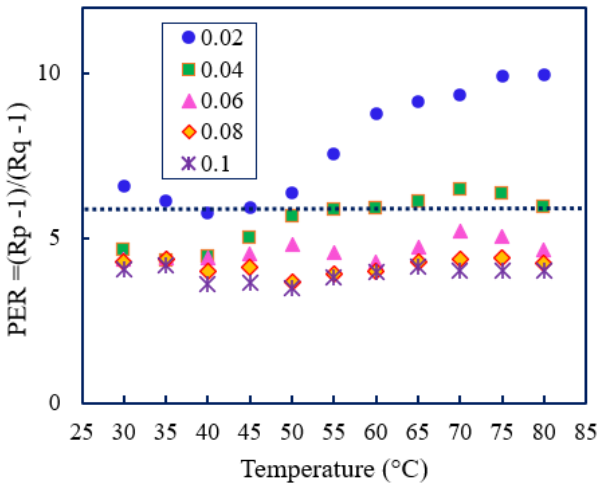

FIGURE 10. Heat transfer efficiency of TiO_2-Al_2O_3 hybrid nanofluids including 40% EG.

the base fluid significantly enhances thermal conductivity, notably enhanced at high-performance limits. In contrast, it is characterized by inordinately high values of PER due to the relatively low improvement in heat conduction at lower particle loadings [71].

One of the most exciting features of the thermal conductivity profile is an improved rate with temperatures at 60°C to 80°C, which several researchers have already observed [72], [73]. These temperature-dependent effects can be associated with several mechanisms: (i) Increased molecular kinetics: High temperatures result in an overall increase in the frequency and energetic collisions between molecules; (ii) Augmentation of Brownian motion, which is application of more incredible thermal energy promotes random moves within nanoparticles, which triggers faster heat transfer as well; and lastly (iii) Interfacial layering-Temperatures above most critical point might impact ordering at nanoparticle-fluid interface hence influences local transport properties [72]. These synergistic effects further increase the heat transfer property, mainly due to better thermal conductivity [74]. This study is consistent with the existing literature on nanofluid performance. Sheikholeslami et al. [75] also reported similar improvements in heat transfer rates with the inclusion of nanoparticle to base fluids TiO_2-Al_2O_3 hybrid nanofluids with 40% EG exhibit a potential role as coolants and lubricants in solid moving systems, such automotive energy management; laminar flow of multiple mechanical components.

The improved heat transfer behavior of TiO_2-Al_2O_3/W-EG hybrid nanofluids (higher thermal conductivities than the base fluid) makes it more attractive for some target applications with specific temperatures. No obstante, para confirmar estos resultados y estudiar completamente su utilidad en la práctica clínica serán necesarios más estudios experimentales. It should be a presage of an all-out assault on the other thermal properties, viscosity, and shear rate dependence. Incorporating these advanced thermal management

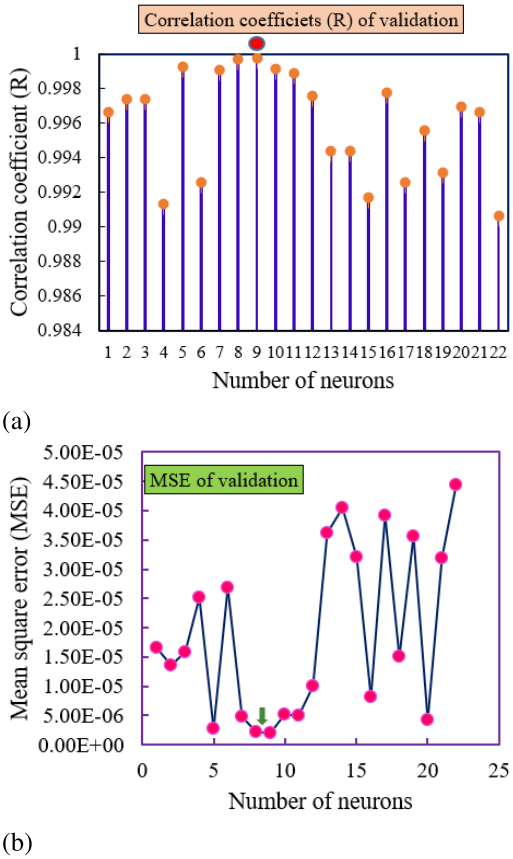

FIGURE 11. (a) MSE values of validation in different numbers of neurons (b) R values of validation for different numbers of neurons.

strategies into real systems offers great potential for energy savings in different industrial sectors.

E. ANN MODEL ANALYSIS

The developed ANN model continually simulates for every number of neurons in the hidden layer. The outcome is computed during each iteration, and the performance of a

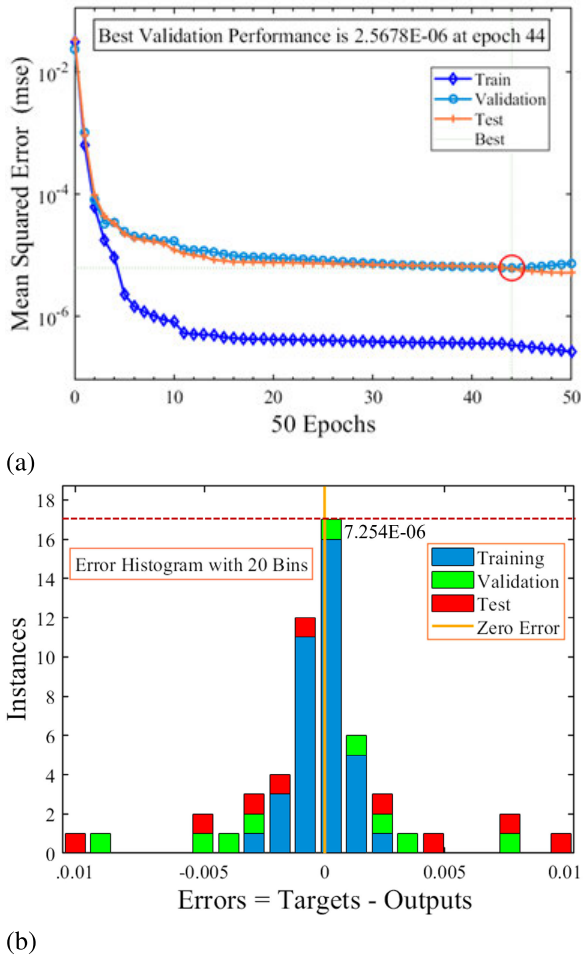

FIGURE 12. (a) Variations in MSE relative to the number of epochs concerning thermal conductivity (b) Error histogram plot.

given neuron number is determined by taking the average value of its performance over all iterations. The number of neurons has been varied in this study from 1 to 22. There are a total of twenty times of inner iterations. Table 5 displays the algorithm's output, ranking the best neuron numbers according to their performance values. All experimental data point performances were calculated, and the train, validation, and test performances were evaluated. The MSE and R are used as evaluation criteria to ensure a comprehensive assessment of the results. Table 5 details the MSE and R values calculated for the train, test, validation, and complete data sets. According to Table 5, the network of 9 neurons in a single hidden layer demonstrates the most favorable overall mean square error and correlation coefficient across the train, validation, test, and all data points. Figures 11(a) and 11(b) show the R and MSE values for the validation plots, which reflect the fluctuations in neurons. In these representations, the R and MSE values corresponding to the ninth neuron are shown by a red circle and a mark, respectively, that looks like an arrow.

Figure 12(a) demonstrates the performance of the reported training, validation, and testing data. The MSE values are shown to decline and stabilize with time as the number of epochs increases. This serves as an exemplification of the effective training undergone by the implemented network. The consistent behavior of mean squared errors with successive increases in epochs also verifies the model's non-overfitting characteristic. At epoch 44, the mean squared error value found to be the smallest within the validation data set was 2.5678×10^{-6}.

Other indications for effective ANN training include the regression diagram and the correlation coefficient between the output data and the desired values. Figure 12(b) presents a comparative analysis of error histograms, providing an insightful assessment of the efficacy of the developed ANN model. The ANN model's entire error spectrum has been partitioned into 20 segments or bin bars, with the horizontal axis depicting the error values and the vertical axis representing the frequency or count of errors relative to the target value. Furthermore, the distinct delineation of the blue, deep orange, and light green bars within the figure represents the training, validation, and testing datasets. A prominent pattern emerges with increased data errors concentrated near the zero point, gradually diminishing as the distance from this point extends. Notably, the heightened numerical density observed in the bar charts adjacent to the zero-error point substantiates the successful predictive capacity of the chosen ANN model, exemplifying an adaptable error distribution centered around zero.

Figure 13 presents the predicting output values against target values for the thermal conductivity parameters, with correlation coefficients of 0.99985, 0.99957, 0.99943, and 0.99961 for the train, test, validation, and complete datasets. The regression diagram depicts the ANN's desired outcomes along the horizontal axis and actual outcomes along the vertical axis. The regression diagram achieves optimal when the ANN's output precisely matches the target value. It results in points perfectly aligned along the bisector line with a unit slope and a correlation coefficient of 1. The obtained regression graphs reveal that the slope value is close to 1. Notably, as unity denotes the ideal slope value in the diagram, the close alignment of the output results with the target becomes apparent, especially considering the test results illustrated in Figure 8. The presence of any form of overfitting within the network would hinder its ability to accurately predict these parameters, as networks affected by overfitting tend to perform well during training and validation but exhibit shortcomings when tested on new data.

In Figure 14, the depiction illustrates the gradual advancement of the gradient in pursuit of a minor cost function (uniformity) across a range of validation assessments, where the gradient is recorded at 1.8802×10^{-7} during the epoch 50, with training extending to 6 at the same epoch. The magnitude of the gradient, coupled with the extent of the validation checks, serves as the criteria for terminating the training process. Notably, the minute value of the gradient suggests minimal performance during training. At the same time, the range of validation checks indicates the number

TABLE 5. The variation of MSE and R with neurons in the hidden layer.

	Training		Testing		Validation	
Neuron	MSE	R	MSE	R	MSE	R
1	1.37940×10^{-5}	0.995740	1.65565×10^{-5}	0.996626	1.35528×10^{-5}	0.997509
2	1.95030×10^{-5}	0.994770	1.35012×10^{-5}	0.997389	1.37692×10^{-5}	0.997038
3	7.17103×10^{-6}	0.998093	1.58016×10^{-5}	0.997366	5.19402×10^{-6}	0.997133
4	6.89959×10^{-6}	0.998239	2.50995×10^{-5}	0.991356	1.61914×10^{-5}	0.993331
5	9.82330×10^{-6}	0.997583	2.69348×10^{-5}	0.999228	1.13725×10^{-5}	0.998538
6	4.75293×10^{-6}	0.998781	2.68440×10^{-5}	0.992564	6.15856×10^{-5}	0.969999
7	1.94986×10^{-6}	0.999419	4.86717×10^{-6}	0.999096	1.22346×10^{-5}	0.997261
8	2.31259×10^{-6}	0.999400	2.24492×10^{-6}	0.999387	2.13943×10^{-5}	0.995738
9	4.86256×10^{-7}	0.999857	7.25415×10^{-6}	0.999435	2.54059×10^{-6}	0.999751
10	2.23419×10^{-6}	0.999365	5.22028×10^{-6}	0.999144	7.70100×10^{-6}	0.997604
11	1.26075×10^{-6}	0.999566	4.95290×10^{-6}	0.998895	9.79321×10^{-6}	0.999001
12	2.00945×10^{-6}	0.999409	1.01050×10^{-5}	0.997562	9.02816×10^{-6}	0.996139
13	3.30219×10^{-6}	0.999029	3.61435×10^{-5}	0.994411	3.16324×10^{-5}	0.994904
14	1.72790×10^{-5}	0.995675	4.05356×10^{-5}	0.994376	1.54583×10^{-4}	0.920851
15	5.59289×10^{-6}	0.998570	3.21607×10^{-5}	0.991701	1.18747×10^{-4}	0.959850
16	1.58892×10^{-7}	0.999954	8.22496×10^{-6}	0.997733	1.97828×10^{-5}	0.997564
17	9.22571×10^{-6}	0.997025	3.91662×10^{-5}	0.992597	2.85060×10^{-5}	0.998496
18	5.55341×10^{-6}	0.998555	1.50717×10^{-5}	0.995601	4.53887×10^{-5}	0.992574
19	7.12550×10^{-6}	0.998267	3.56499×10^{-5}	0.993165	6.98192×10^{-5}	0.984847
20	1.54684×10^{-7}	0.999967	4.31705×10^{-6}	0.996936	4.58234×10^{-5}	0.991143
21	1.08248×10^{-7}	0.999975	3.18580×10^{-5}	0.996629	6.31909×10^{-5}	0.991473
22	2.29464×10^{-5}	0.994498	5.43203×10^{-5}	0.990625	1.49282×10^{-4}	0.946996

TABLE 6. Weights and biases for the thermal conductivity prediction.

Neurons	Hidden layer			Output layer	
	Weights		Biases	Weights	Biases
	VC	T			
1	10.182	7.903	-12.520	-0.131	0.318
2	-9.927	-8.258	12.331	-0.657	
3	0.299	-13.474	-10.098	-0.165	
4	11.775	-7.243	-8.538	-0.138	
5	-5.184	12.178	7.9903	-0.004	
6	-13.418	-0.415	6.313	-0.238	
7	-12.677	1.773	6.233	-0.253	
8	10.816	-8.048	-3.408	-0.247	
9	12.972	2.027	-3.164	-0.011	
10	7.309	10.129	-1.081	-0.235	
11	10.800	7.186	-1.141	0.460	
12	-11.999	4.911	-1.657	-0.534	
13	-9.057	9.445	-2.116	-0.144	
14	-7.174	11.200	-2.198	0.136	
15	-11.842	5.608	-4.980	0.480	
16	-7.627	-10.829	-5.347	0.150	
17	2.885	-12.740	6.858	-0.088	
18	-2.364	-12.967	-8.022	-0.002	
19	13.578	-3.287	8.077	0.237	
20	-11.863	-5.072	-11.072	-0.354	
21	4.951	11.878	12.068	-0.061	
22	-8.067	-10.348	13.202	-0.131	

of consecutive iterations wherein the validation performance fails to demonstrate any reduction.

Figure 15 illustrates a comprehensive comparison between the thermal conductivity values obtained from the ANN model and the experimental data conducted across varying volume concentrations of the hybrid nanofluid at different temperatures. Notably, the findings reveal the remarkable precision the current ANN model exhibited in accurately predicting thermal conductivity, with the observed deviation from the experimental data remaining under 1. Table 6 outlines the weights and biases associated with the developed ANN model. The observations indicate a continuous modification of weights and biases with an increasing number of neurons, underscoring the influence of input parameters on the output variables. Notably, at the ninth neuron, the alterations in weights and biases become negligible, suggesting that input changes have minimal impact on the network's output. Consequently, the configuration of 9 neurons within the hidden layer appears well-suited for the network's operations.

F. SVM MODEL ANALYSIS

Like the ANN, the precision of the SVR model was evaluated by examining the MSE and R values, comparing the predicted and experimental relative thermal conductivity outcomes. The values for the MSE and R are computed to evaluate the model's accuracy in predicting the thermal conductivity of the Al_2O_3/TiO_2 hybrid nanofluid using Equations (8) and (9). Table 7 and Figures 16 and 17 provide the statistical and graphical result. The statistical findings obtained for the model's training and validation phases are illustrated in Table 7. The results reveal a significantly high correlation coefficient and minimal MSE values, suggesting the robust computational efficacy of the developed model in predicting thermal conductivity. According to the data presented in Table 8, the training dataset demonstrates a high correlation coefficient with an R-value of 0.9964, indicating substantial agreement between experimental and predicted values during training. On the other hand, the R-value for the validation dataset was found to be 0.9916, slightly surpassing the training set by 0.0048. Despite this marginal difference, the findings still denote a satisfactory performance of the prediction model.

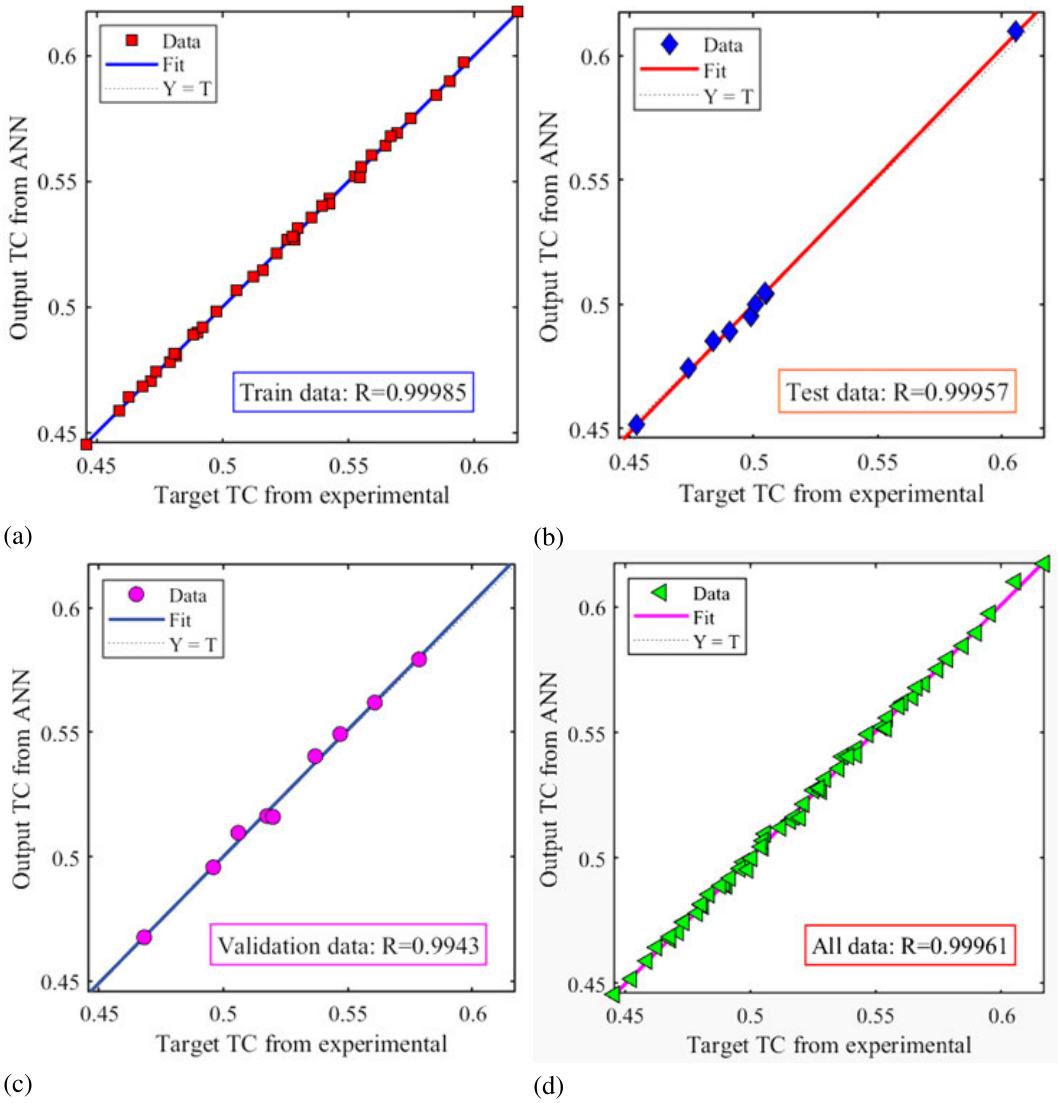

FIGURE 13. Regression diagram and the correlation coefficient between the actual output values and target values.

TABLE 7. Optimum outcomes of SVM model.

	Training	Validation
RMSE	0.0036051	0.0046191
R	0.9964	0.9916
MSE	1.2667×10^{-5}	2.1336×10^{-5}
MOD	1.5%	1.6%

Figure 17 provides a visual representation of the validation model, indicating a uniform distribution of errors around the zero line. This observation underscores the effectiveness of the SVR as a robust predictive model for accurately determining the thermal conductivity of nanofluids. Figure 17(a) compares the experimental and predicted values obtained using the SVR model. The conspicuous alignment between the projected and measured values of the thermophysical characteristics is evident across all parameters, emphasizing the model's robust and accurate predictive capacity. The MSE values effectively underscore the formidable and dependable performance demonstrated by the SVR model, precisely estimating each thermophysical property with high accuracy and reliability. Figure 17(b) shows the residual plot of the SVM method.

G. CURVE FITTING ANALYSIS

Utilizing a curve-fitting approach, a comprehensive analysis of the experimental data led to the generation of a curve, showcasing optimal results by applying functions of varying orders. Consequently, the third-order function for volume fraction and a second-order function for temperature yielded the most accurate fit. This best fit is expressed in Eq. (26), the linear model Poly32, as outlined in reference [75]. The fitted curve is represented as Eq. (20).

$$\begin{pmatrix} \int(m,n) = g_{00} + g_{10}(m) + g_{01}(n) \\ +g_{20}(m)^2 + g_{11}(m\times n) + g_{02}(n)^2 \\ +g_{30}(m)^3 + g_{21}(m^2\times n) + g_{12}(m\times n^2) \end{pmatrix} \tag{20}$$

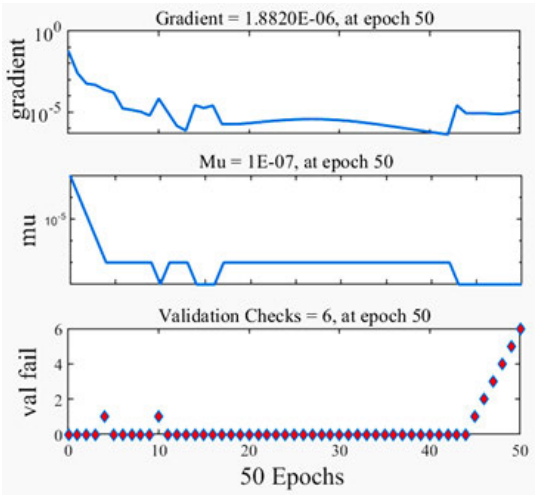

FIGURE 14. Gradient progression.

In Equation (20), the variables $'m'$ and $'n'$ denote nanoparticles' temperature and volume fraction, respectively, with the corresponding coefficients detailed in Table 8. The various mechanisms and phenomena involved in the thermal conductivity enhancement in the TiO_2-Al_2O_3/water-EG hybrid nanofluid system featured in this work have been thoroughly supported by robust curve-fitting analysis results ($R = 0.9964$; $MSE = 7.475 \times 10^{-5}$ and an $RMSE = 8.6458 \times 10^{-3}$). The non-linear increase in thermal conductivity with temperature is observed due to the rise in the Brownian motion at higher temperatures, which causes more frequent collisions between particles and thus transfers the heat. The fluid viscosity, a response to the temperature elevation from the generated heat, becomes lower. Thus, the particle can disperse better, and the thermal transport is improved. The observed augmentations of thermal conductivities of the nanofluids with increasing volume concentrations are consistent with Maxwell's effective medium theory, and the much higher enhancements compared with those of the corresponding mono-nanofluids may be due to the use of particle size distributions that are complementary and, therefore, optimum surface area-to-volume ratios. The optimal performance at 0.2% volume concentration supports previous findings from Hamid et al. [32], who recognized comparable optimization opportunities within hybrid systems, attributing to the balance between enhanced thermal transport and greater viscosity at higher concentrations. The peaks in UV-Vis spectra for 0.10% and 0.2% concentrations (Figure 18) show that electrostatic repulsion, steric hindrance, and optimization of particle surface chemistry at expected high concentrations provide optimal dispersion stability. These curvilinear fits are made possible with extraordinary curve-fitting parameters ($R = 0.9964$; $MSE = 7.475 \times 10^{-5}$) and an $RMSE = 8.6458 \times 10^{-3}$) shows that our model reliability is much better than previous work. They reported lower values of R in their analysis of thermal conductivity. Such results provide

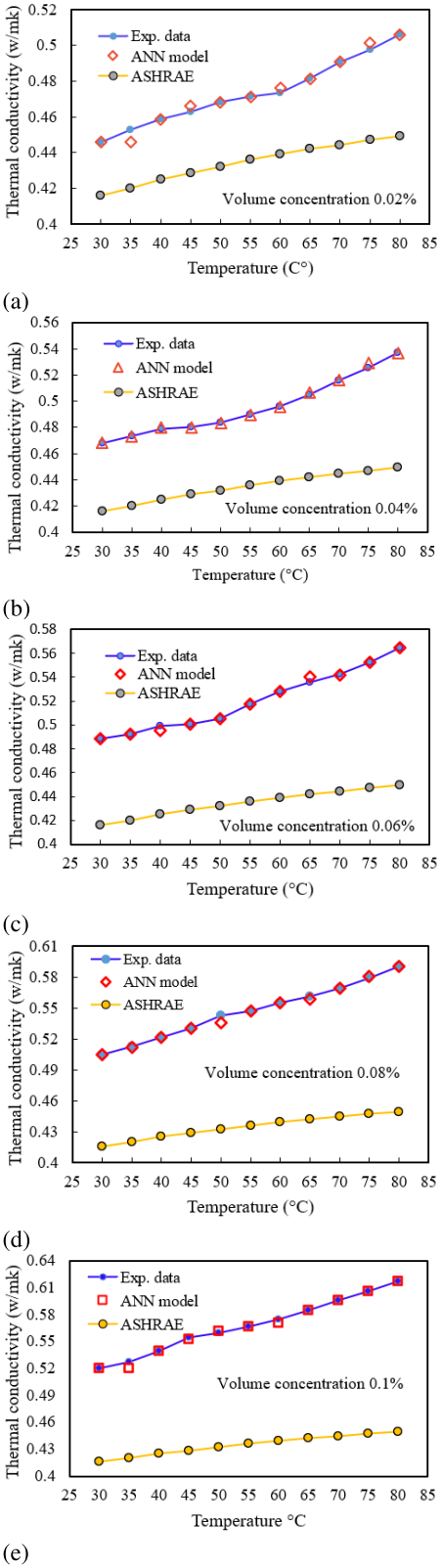

FIGURE 15. Equality plot of thermal conductivity at (a) 0.02 (b) 0.04 (c) 0.06 (d) 0.08 and (e) 0.10 volume concentration with changing temperature.

a promising viewpoint on applying hybrid systems for practical thermal management technology, yet also indicate

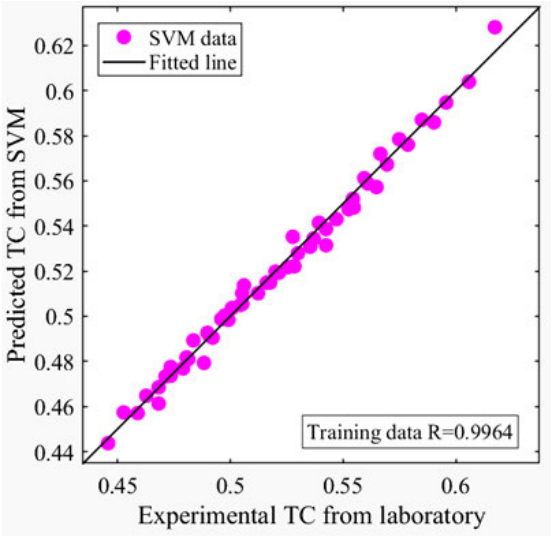

FIGURE 16. (a) Regression plot of thermal conductivity for (a) training data (b) validation data.

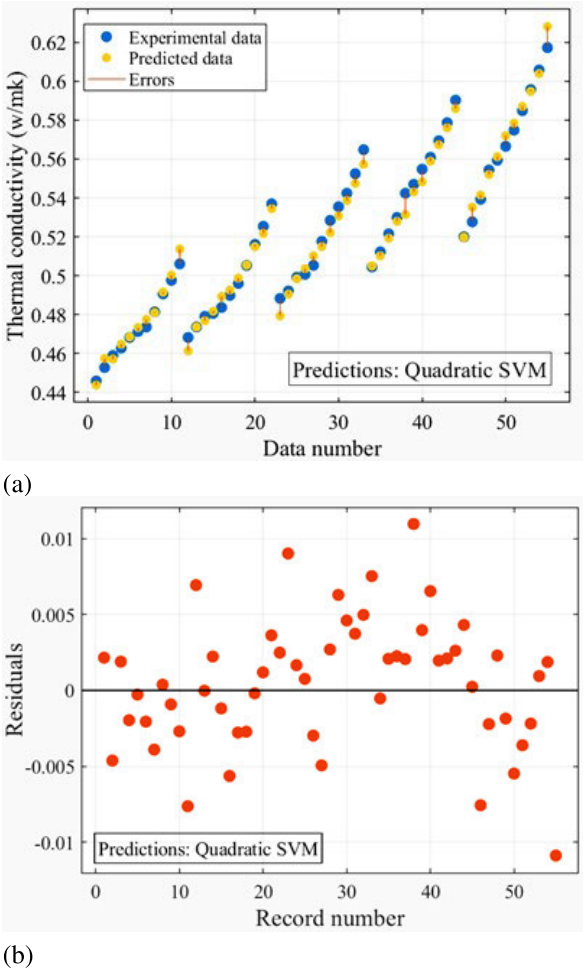

FIGURE 17. (a) Regression plot of thermal conductivity for (a) training data (b) validation data.

TABLE 8. Coefficient values of CF.

Coefficient	value	Coefficient	value
g_{00}	0.4871	g_{02}	16.75
g_{10}	-1.024	g_{30}	0.0393
g_{01}	-0.001932	g_{21}	2.463×10^{-5}
g_{20}	-85.36	g_{12}	-0.02591
g_{11}	-0.000232		

future work needed, such as long-term stability, development of more advanced predictive modeling, ratio optimization for applications, and cost assessments for the industry. This synergy between temperature and concentration, the increase in particle movement and interaction, and the effect of localized structures and nanolayer formation can be useful for exploring and optimizing next-generation thermal management.

V. PERFORMANCE COMPARISON AMONG DIFFERENT MODELS

The thermal conductivity was calculated using these models to assess the prediction accuracy of the current analytical models (ANN, CF, and SVM) concerning the measured data of Al_2O_3 and TiO_2 hybrid nanofluid. The resultant model outputs were graphically represented in a bar graph displayed in Figure 19(a). Furthermore, Figure 19(a)(a-c) presents periodic depictions comparing these models' MSE, RMSE, and R values. It is observed from these graphs that MSE and RMSE values are lowest for the ANN model compared to other models. However, the R-value of the ANN model is higher than the SVM and CF models. The lowest MSE, RMSE, and highest R are the obligatory conditions for building the best model for the best performance. Consequently, the ANN employing the LM learning function demonstrated the closest agreement with the experimental data. Nevertheless, the SVR approach also exhibited impeccable prediction, albeit with a slight tendency to overestimate compared to the ANN. Comparing these

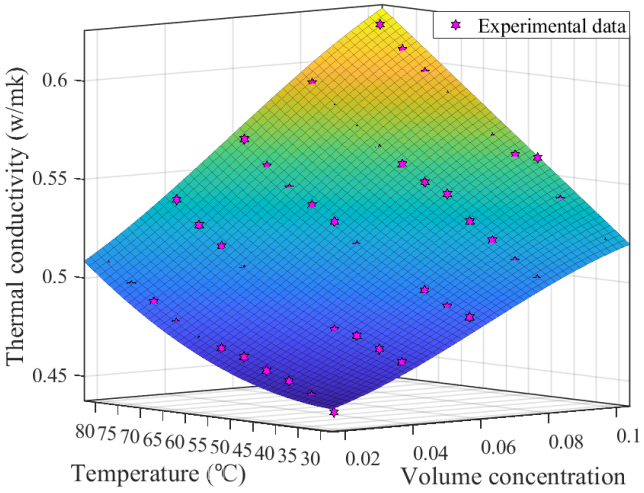

FIGURE 18. The fitted curve.

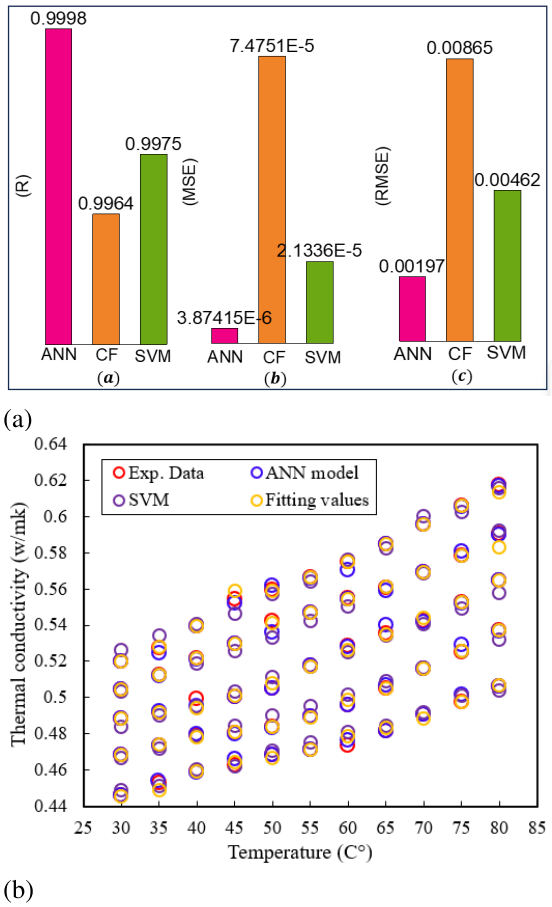

FIGURE 19. (a) Experimental, ANN, SVM and CF outputs (b) Performance comparison of ANN, CF, and SVM models with the parameters of (a) R, (b) MSE, and (c) RMSE.

three models, CF presented the lowest performance as his MSE and RMSE values are higher, and the R-value is lower than ANN and SVM models. Figure 19(b) compares the experimental data and the results predicted by the models. The experimental data and various model outputs exhibit

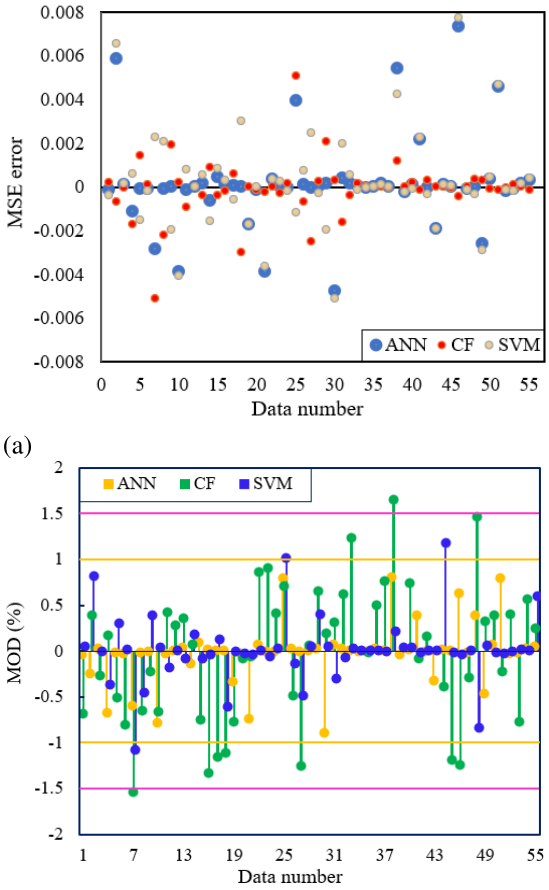

FIGURE 20. (a) Error comparison (b) MOD comparison among the ANN, CF, and SVM.

strong coherence; notably, the ANN model outperforms the others, underscoring the commendable performance of the employed neural network.

The results of the ANN, CF, and SVM models' errors are depicted in Figure 20(a). The clustering of errors around the zero line proves the models' exceptional performance. Furthermore, the error rate of the ANN notably surpasses that of the SVM and CF methods. Similarly, Figure 20(b) provides a graphic representation of the MOD range across the ANN, CF, and SVM models. The graph shows that the maximum MOD value for the ANN model is close to 1%. On the contrary, the MOD value of SVM is approximately 1.5%, whereas FC exceeds this range. The minimal MOD value achieved by the ANN model signifies its robust performance compared to the other models, demonstrating exceptional quality and dependability in its application.

For a more detailed assessment of the ability of the applied models to predict thermal conductivity separately a Taylor diagram is presented in Figure 21. It is a handy tool to visualize how well the model performs over different depths, showing simultaneously correlation coefficient and standard deviation together with centered RMSE. The resulting Taylor

TABLE 9. Summary of some studies in ANN/ SVM methods.

Ref.	Nanofluids	Input	Output	Accuracy	Network configuration	Model
[76]	Fe_3O_4/water	Temperature, volume fraction	Thermal conductivity, zeta potential	R=0.99 MSE=1.47×10^{-5}	2-7-1, 2-9-1, Tansig, purlin	MLP
[77]	TiO_2–water	Temperature, volume concentration, size, and shape of NF	Thermal conductivity	R=0.99 MSE= 0.0003	4-12-12-12-1 ReLu, linear LM	ANN
[78]	MWCNT /EG	Temperature, volume concentration	Thermal conductivity	R= 0.993 MSE= 1.9×10^{-5}	2-6-1,Tansig, purlin, LM	ANN
[81]	MWCNT-Fe_3O_4/ water	volume fraction, average size, temperature	Thermal conductivity	R= 0.997 MSE=1.060×10^{-4}	5-fold cross-validation	LSSVM
[82]	MWCNTs, titania, zinc oxide/W-EG	temperature, volume concentration	thermal characteristics	R=0.9972 MSE=4.08×10^{-6}	Polynomial	CF
[83]	WO_3-CuO-Ag/ Water	Temperature, volume concentration	Thermal conductivity	R=0.9988 MSE=0.0086941	2-8-1, Logsig, purlin, LM	MLP
[84]	CuO-GNP-Al_2O_3 /water-EG	Temperature, volume fraction (water, EG, CuO, GNP, Al2O3)	Thermal conductivity, viscosity	R= 0.9949 MSE= 0.00057	7-9-2, sigmoid Purlin, LM	ANN
[85]	Al_2O_3/ engine oil	Temperature, volume concentration, share rate	viscosity	R=0.9958 MSE=4.1446×10^{-8}	3-6-4-1,Sigmoid, linear, LM	FFNN
[86]	GO-CuO/ water-EG	Temperature, volume fraction, share rate	viscosity	R=0.9950 MSE= 0.0125	3-10-1, Sigmoid Purlin, LM	ANN
[87]	MWCNT, MgO	shear rate, temperature, solid concentration	Dynamic viscosity	R= 0.9999 RMSE=0.783	RBF, Bayesian	LSSVM
Present work	Al_2O_3, TiO_2	temperature, volume concentration	Thermal conductivity	R=0.9998 MSE=3.87×10^{-6}	2-9-1, sigmoid, purlin, LM	ANN
Present work	Al_2O_3, TiO_2	temperature, volume concentration	Thermal conductivity	R=0.9916 MSE=2.13×10^{-5}	5-fold cross-validation	SVM
Present work	Al_2O_3, TiO_2	temperature, volume concentration	Thermal conductivity	R=0.9964, MSE=7.47×10^{-5}	Polynomial	CF

diagram shows that the estimation of the ANN model is more reliable and smoother than that of SVM or CF (Curve fitting) models with higher accuracy. Figure 21 shows the test sample and class of output that greater distance between points shows superiority, which is also exhibited by the point to a target; the ANN model comes closer from further away than other nearest neighbors, which is a more coherent and better generalization. In the comparison, SVM queues up at second performance compared with CF. This is compared to the standard deviation of observed values of 0.043 for thermal conductivity. It allows us to get a rough estimate of our experimental data variable and provides some context for the accuracy with which models can make predictions. Improved comprehension of model performance using the Taylor diagram in this analysis represents a detailed insight that can be used predictively to assign these tools for thermal conductivity estimation on similar systems.

This section also covers our proposed method and some other method's performance, as shown in Table 9. Hence, R and MSE are considered as performance metrics. A recently proposed method [76] using ANN to predict the thermal conductivity with R above 0.99 and MSE 1.47×10^{-5}. Another technique in [77] predicts thermal conductivity with 0.99 of R and 0.0003 of MSE. The authors in [78] got R = 0.993 and MSE = 1.9×10^{-5} for thermal

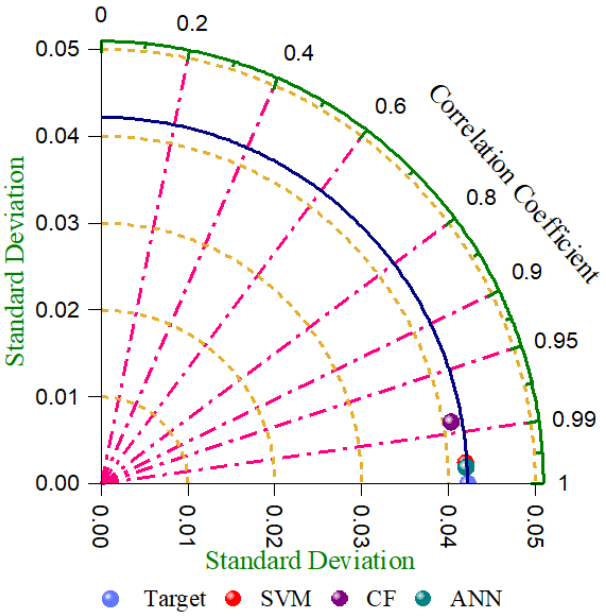

FIGURE 21. Taylor diagram of the predicted thermal conductivity values.

conductivity prediction with the ANN method. In [79] the author used ANN and achieved 0.9964 and 2.20×10^{-6} for R and MSE to predict the thermal conductivity. The

paper in [80] used SVM for thermal conductivity prediction where R and RMSE were 0.97 and 1.46. To predict thermal conductivity, Hassan et al. [81] found R = 0.997 and MSE = 1.060×10^{-4} using LSSVM. Some articles used the CF method and compared it with the ANN method. For example, in [86], predict thermal conductivity using CF and ANN where R and MSE are 0.9972 and 4.08×10^{-6} for CF and 0.9951 and 2.0402×10^{-5} for ANN model. Another research study [32] found R and MSE values of 0.9983 and 4.0223 using CF to predict thermal conductivity. In contrast, our research acquired the R and MSE 0.9998 and 3.874×10^{-5} for ANN, 0.9975 and 2.1336×10^{-5} for SVM, and 0.9964 and 7.475×10^{-5} for CF.

VI. CONCLUSION

The thermal conductivity of a hybrid nanofluid, synthesized as consisting of water/ethylene glycol (EG)-based Al_2O_3 and TiO_2 are examined in this research. This study uses the nanofluid's thermal properties to investigate the influences of different volume concentrations (0.02% to 0.1%) and temperatures ranging from 30–80 °C. The stability of the 60:40 W/EG-based $TiO_2 - Al_2O_3$ hybrid nanofluid was examined via visual sedimentation photography, UV-Vis spectral study, and zeta potential measurements. The main results emerged from this work:

1) The experimental results obtained using three different methods imply the good stability of as-prepared nanofluids over a duration longer than two weeks. Meanwhile, the thermal conductivity of nanofluids is proportional to temperature and particle concentration at the same time. In the most substantial concentration (0.1%) and at this case, i.e., 80 °C, a maximum increase of 40.86 % is attained in thermal conductivity; the temperature has more impact on nanofluids with higher concentrations. It can be seen that the thermal conductivity of TiO_2-Al_2O_3 hybrid nanofluids at all concentrations is higher than single-component TiO_2 and Al_2O_3.
2) Determination of the performance enhancement ratio of the nanofelds, based on thermal conductivity improvement, illustrated a characteristic profile for heat transfer applications where optimal significance in thermal conductivities was derived. Nanofluids available at concentrations greater than 0.04% can offer higher heat transfer capabilities, suggesting they may be suited to thermal management systems. The prepared nanofluids' thermal behavior and stability characteristics have been interpreted based on these results, showing promises for several heat transfer applications with such improved properties and improvement possibilities to enhance significantly heat transport efficiency in engineered systems.
3) An ANN technique is proposed, leveraging the empirical data to strategically adjust the neurons within the hidden layer, identifying an optimal model with nine neurons. Notably, implementing the LM algorithm as the training function, coupled with the utilization of 'tansig' and 'purelin' functions in the hidden and output layers, respectively, showcases a meticulously tailored and refined methodology for enhanced predictive accuracy and model performance. The achieved MSE and R values were 4.86256×10^{-6} 2.54059×10^{-6}, 7.25415×10^{-6} and 0.99985, 0.99957, and 0.99961 for training, testing, and validation periodically.
4) The laboratory data was analyzed by implementing the ANN model alongside applying other intelligent methodologies such as SVM. The R values obtained from these methods were calculated as 0.9975 and 0.9964, with corresponding MSE values of 1.27 × 10-5 and 2.831 × 10-5 for training and validation, respectively.
5) A CF method was also successfully applied in this study where obtained R and MSE were 0.9964 and 7.4575×10^{-5}, respectively.
6) The comparative analysis demonstrated the superior predictive capability of the ANN model, evidenced by an impressive overall R-value of 0.9998 and an MSE of 3.8741×10^{-6}. Further validation by comparing the ANN model's output with the experimental data confirmed an excellent agreement, with deviations falling below 1%.

This study contributes to the advancement of predictive modeling in thermal conductivity analysis and highlights the potential applications of the developed ANN model in various industrial and research contexts. This study was carried out to contribute to the advancement of predictive modeling in thermal conductivity analysis. Our future objective is to explore significant and multi-label datasets to assess the proposed method and enhance the model's generalization capabilities.

ACKNOWLEDGMENT

The authors extend their appreciation to Universiti Malaysia Pahang Al-Sultan Abdullah, Malaysia, for their provision of laboratory facilities and financial assistance.

REFERENCES

[1] J. Gao, H. Chen, Y. Li, J. Chen, Y. Zhang, K. Dave, and Y. Huang, "Fuel consumption and exhaust emissions of diesel vehicles in worldwide harmonized light vehicles test cycles and their sensitivities to eco-driving factors," *Energy Convers. Manage.*, vol. 196, pp. 605–613, Sep. 2019, doi: 10.1016/j.enconman.2019.06.038.

[2] S. Nasreen, M. B. Mbarek, and M. Atiq-ur-Rehman, "Long-run causal relationship between economic growth, transport energy consumption and environmental quality in Asian countries: Evidence from heterogeneous panel methods," *Energy*, vol. 192, Feb. 2020, Art. no. 116628, doi: 10.1016/j.energy.2019.116628.

[3] A. Kaleli, "Development of the predictive based control of an autonomous engine cooling system for variable engine operating conditions in Si engines: Design, modeling and real-time application," *Control Eng. Pract.*, vol. 100, Jul. 2020, Art. no. 104424, doi: 10.1016/j.conengprac.2020.104424.

[4] H. W. Xian, N. A. C. Sidik, and R. Saidur, "Hybrid nanocoolant for enhanced heat transfer performance in vehicle cooling system," *Int. Commun. Heat Mass Transf.*, vol. 133, Apr. 2022, Art. no. 105922, doi: 10.1016/j.icheatmasstransfer.2022.105922.

[5] Y. Shang, K. A. Hammoodi, A. Alizadeh, K. Sharma, D. J. Jasim, H. Rajab, M. Ahmed, M. Kassim, H. Maleki, and S. Salahshour, "Artificial neural network hyperparameters optimization for predicting the thermal conductivity of MXene/graphene nanofluids," *J. Taiwan Inst. Chem. Engineers*, vol. 164, Nov. 2024, Art. no. 105673, doi: 10.1016/j.jtice.2024.105673.

[6] I. Wole-Osho, E. C. Okonkwo, H. Adun, D. Kavaz, and S. Abbasoglu, "An intelligent approach to predicting the effect of nanoparticle mixture ratio, concentration and temperature on thermal conductivity of hybrid nanofluids," *J. Thermal Anal. Calorimetry*, vol. 144, no. 3, pp. 671–688, May 2021, doi: 10.1007/s10973-020-09594-y.

[7] L. Yang, W. Ji, M. Mao, and J.-N. Huang, "An updated review on the properties, fabrication and application of hybrid-nanofluids along with their environmental effects," *J. Cleaner Prod.*, vol. 257, Jun. 2020, Art. no. 120408, doi: 10.1016/j.jclepro.2020.120408.

[8] H. Eshgarf, R. Kalbasi, A. Maleki, M. S. Shadloo, and A. Karimipour, "A review on the properties, preparation, models and stability of hybrid nanofluids to optimize energy consumption," *J. Thermal Anal. Calorimetry*, vol. 144, no. 5, pp. 1959–1983, Jun. 2021, doi: 10.1007/s10973-020-09998-w.

[9] A. H. Pordanjani, S. Aghakhani, M. Afrand, M. Sharifpur, J. P. Meyer, H. Xu, H. M. Ali, N. Karimi, and G. Cheraghian, "Nanofluids: Physical phenomena, applications in thermal systems and the environment effects—A critical review," *J. Cleaner Prod.*, vol. 320, Oct. 2021, Art. no. 128573, doi: 10.1016/j.jclepro.2021.128573.

[10] X. Li, H. Wang, and B. Luo, "The thermophysical properties and enhanced heat transfer performance of SiC-MWCNTs hybrid nanofluids for car radiator system," *Colloids Surf. A, Physicochemical Eng. Aspects*, vol. 612, Mar. 2021, Art. no. 125968, doi: 10.1016/j.colsurfa.2020.125968.

[11] F. Abbas, H. M. Ali, T. R. Shah, H. Babar, M. M. Janjua, U. Sajjad, and M. Amer, "Nanofluid: Potential evaluation in automotive radiator," *J. Mol. Liquids*, vol. 297, Jan. 2020, Art. no. 112014, doi: 10.1016/j.molliq.2019.112014.

[12] S. Jana, A. Salehi-Khojin, and W.-H. Zhong, "Enhancement of fluid thermal conductivity by the addition of single and hybrid nano-additives," *Thermochimica Acta*, vol. 462, nos. 1–2, pp. 45–55, Oct. 2007, doi: 10.1016/j.tca.2007.06.009.

[13] V. Kumar and R. R. Sahoo, "Exergy and energy performance for wavy fin radiator with a new coolant of various shape nanoparticle-based hybrid nanofluids," *J. Thermal Anal. Calorimetry*, vol. 143, no. 6, pp. 3911–3922, Mar. 2021, doi: 10.1007/s10973-020-09361-z.

[14] F. C. Nagarajan, S. K. Kannaiyan, and C. Boobalan, "A proficient approach to enhance heat transfer using cupric oxide/silica hybrid nanoliquids," *J. Thermal Anal. Calorimetry*, vol. 147, no. 10, pp. 5589–5598, May 2022, doi: 10.1007/s10973-021-10956-3.

[15] A. Kumar, P. Chand, and M. A. Hassan, "Louvered finned car radiator with MWCNT-SiO_2 hybrid nanofluid: An experimental approach," *Powder Technol.*, vol. 415, Feb. 2023, Art. no. 118176, doi: 10.1016/j.powtec.2022.118176.

[16] A. Dunga, R. Koona, and S. V. Naidu, "Experimental investigation of thermal conductivity of alumina (Al_2O_3)-Multi-Walled carbon nanotubes (MWCNT) in water-ethylene glycol hybrid nanofluid," *J. Nanofluids*, vol. 11, no. 1, pp. 58–73, Feb. 2022, doi: 10.1166/jon.2022.1820.

[17] M. Baghoolizadeh, D. J. Jasim, S. M. Sajadi, R. R. Renani, M. R. Renani, and M. Hekmatifar, "Using of artificial neural networks and different evolutionary algorithms to predict the viscosity and thermal conductivity of silica-alumina-MWCN/water nanofluid," *Heliyon*, vol. 10, no. 4, 2024, Art. no. 26279, doi: 10.1016/j.heliyon.2024.e26279.

[18] M. M. Hasan, M. S. Islam, S. A. Bakar, M. M. Rahman, and M. N. Kabir, "Applications of artificial neural networks in engine cooling system," in *Proc. Int. Conf. Softw. Eng. Comput. Syst. 4th Int. Conf. Comput. Sci. Inf. Manage.*, Aug. 2021, pp. 471–476.

[19] A. M. Alklaibi, K. V. V. C. Mouli, and L. S. Sundar, "Heat transfer, and friction factor of Fe_3O_4–SiO_2/water hybrid nanofluids in a plate heat exchanger: Experimental and ANN predictions," *Int. J. Thermal Sci.*, vol. 195, Jan. 2024, Art. no. 108608, doi: 10.1016/j.ijthermalsci.2023.108608.

[20] S. Rostami, D. Toghraie, B. Shabani, N. Sina, and P. Barnoon, "Measurement of the thermal conductivity of MWCNT-CuO/water hybrid nanofluid using artificial neural networks (ANNs)," *J. Thermal Anal. Calorimetry*, vol. 143, no. 2, pp. 1097–1105, Jan. 2021, doi: 10.1007/s10973-020-09458-5.

[21] M. Hemmat Esfe, S. Esfandeh, and D. Toghraie, "Investigation of different training function efficiency in modeling thermal conductivity of TiO_2/water nanofluid using artificial neural network," *Colloids Surf. A, Physicochemical Eng. Aspects*, vol. 653, Nov. 2022, Art. no. 129811, doi: 10.1016/j.colsurfa.2022.129811.

[22] S. H. Rostamian, M. Biglari, S. Saedodin, and M. Hemmat Esfe, "An inspection of thermal conductivity of CuO-SWCNTs hybrid nanofluid versus temperature and concentration using experimental data, ANN modeling and new correlation," *J. Mol. Liquids*, vol. 231, pp. 364–369, Apr. 2017, doi: 10.1016/j.molliq.2017.02.015.

[23] A. Pare and S. K. Ghosh, "A unique thermal conductivity model (ANN) for nanofluid based on experimental study," *Powder Technol.*, vol. 377, pp. 429–438, Jan. 2021, doi: 10.1016/j.powtec.2020.09.011.

[24] Y. Peng, A. Parsian, H. Khodadadi, M. Akbari, K. Ghani, M. Goodarzi, and Q.-V. Bach, "Develop optimal network topology of artificial neural network (AONN) to predict the hybrid nanofluids thermal conductivity according to the empirical data of Al_2O_3–Cu nanoparticles dispersed in ethylene glycol," *Phys. A, Stat. Mech. Appl.*, vol. 549, Jul. 2020, Art. no. 124015, doi: 10.1016/j.physa.2019.124015.

[25] M. M. Hasan, M. M. Rahman, M. S. Islam, W. H. Chan, Y. M. Alginahi, M. N. Kabir, S. A. Bakar, and D. Ramasamy, "Artificial neural network modeling for predicting thermal conductivity of EG/water-based CNC nanofluid for engine cooling using different activation functions," *Frontiers Heat Mass Transf.*, vol. 22, no. 2, pp. 537–556, 2024, doi: 10.32604/fhmt.2024.047428.

[26] A. Asadi, A. N. Bakhtiyari, and I. M. Alarifi, "Predictability evaluation of support vector regression methods for thermophysical properties, heat transfer performance, and pumping power estimation of MWCNT/ZnO–engine oil hybrid nanofluid," *Eng. Comput.*, vol. 37, no. 4, pp. 3813–3823, Oct. 2021, doi: 10.1007/s00366-020-01038-3.

[27] M. Hemmat Esfe, S. Ali Eftekhari, A. Alizadeh, S. Aminian, M. Hekmatifar, and D. Toghraie, "A well-trained artificial neural network for predicting the optimum conditions of MWCNT–ZnO (10:90)/ SAE 40 nano-lubricant at different shear rates, temperatures, and concentration of nanoparticles," *Arabian J. Chem.*, vol. 16, no. 2, Feb. 2023, Art. no. 104508, doi: 10.1016/j.arabjc.2022.104508.

[28] W. T. Urmi, M. M. Rahman, W. A. Wan Hamzah, K. Kadirgama, D. Ramasamy, and M. A. Maleque, "Experimental investigation on the stability of 40% ethylene glycol based TiO_2-Al_2O_3 hybrid nanofluids," *J. Adv. Res. Fluid Mech. Thermal Sci.*, vol. 69, no. 1, pp. 110–121, Apr. 2020, doi: 10.37934/arfmts.69.1.110121.

[29] W. Urmi, M. M. Rahman, and W. A. W. Hamzah, "An experimental investigation on the thermophysical properties of 40% ethylene glycol based TiO_2-Al_2O_3 hybrid nanofluids," *Int. Commun. Heat Mass Transf.*, vol. 116, Jul. 2020, Art. no. 104663, doi: 10.1016/j.icheatmasstransfer.2020.104663.

[30] V. Vicki Wanatasanappan, P. Kumar Kanti, P. Sharma, N. Husna, and M. Z. Abdullah, "Viscosity and rheological behavior of Al_2O_3-Fe_2O_3/water-EG based hybrid nanofluid: A new correlation based on mixture ratio," *J. Mol. Liquids*, vol. 375, Apr. 2023, Art. no. 121365, doi: 10.1016/j.molliq.2023.121365.

[31] A. Rehman, S. Yaqub, M. Ali, H. Nazir, N. Shahzad, S. Shakir, R. Liaquat, and Z. Said, "Effect of surfactants on the stability and thermophysical properties of Al_2O_3+TiO_2 hybrid nanofluids," *J. Mol. Liquids*, vol. 391, Dec. 2023, Art. no. 123350, doi: 10.1016/j.molliq.2023.123350.

[32] K. A. Hamid, W. H. Azmi, M. F. Nabil, R. Mamat, and K. V. Sharma, "Experimental investigation of thermal conductivity and dynamic viscosity on nanoparticle mixture ratios of TiO_2-SiO_2 nanofluids," *Int. J. Heat Mass Transf.*, vol. 116, pp. 1143–1152, Jan. 2018, doi: 10.1016/j.ijheatmasstransfer.2017.09.087.

[33] M. F. Nabil, W. H. Azmi, K. Abdul Hamid, R. Mamat, and F. Y. Hagos, "An experimental study on the thermal conductivity and dynamic viscosity of TiO_2-SiO_2 nanofluids in water: Ethylene glycol mixture," *Int. Commun. Heat Mass Transf.*, vol. 86, pp. 181–189, Aug. 2017, doi: 10.1016/j.icheatmasstransfer.2017.05.024.

[34] H. Setia, R. Gupta, and R. K. Wanchoo, "Stability of nanofluids," *Mater. Sci. Forum*, vol. 757, pp. 139–149, May 2013, doi: 10.4028/www.scientific.net/msf.757.139.

[35] A. Asadi, M. Asadi, A. Rezaniakolaei, L. A. Rosendahl, M. Afrand, and S. Wongwises, "Heat transfer efficiency of Al_2O_3-MWCNT/thermal oil hybrid nanofluid as a cooling fluid in thermal and energy management applications: An experimental and theoretical investigation," *Int. J. Heat Mass Transf.*, vol. 117, pp. 474–486, Feb. 2018, doi: 10.1016/j.ijheatmasstransfer.2017.10.036.

[36] A. I. Ramadhan, W. H. Azmi, R. Mamat, K. A. Hamid, and S. Norsakinah, "Investigation on stability of tri-hybrid nanofluids in water-ethylene glycol mixture," *IOP Conf. Ser., Mater. Sci. Eng.*, vol. 469, Jan. 2019, Art. no. 012068.

[37] J. M. P. França, S. I. C. Vieira, M. J. V. Lourenço, S. M. S. Murshed, and C. A. Nieto de Castro, "Thermal conductivity of $[C_4mim][(CF_3SO_2)_2N]$ and $[C_2mim][EtSO_4]$ and their IoNanofluids with carbon nanotubes: Experiment and theory," *J. Chem. Eng. Data*, vol. 58, no. 2, pp. 467–476, Feb. 2013, doi: 10.1021/je301183r.

[38] *ASHRAE Handbook-Fundamentals-Chapter 30-Materials*, GA, USA, 2009.

[39] V. V. Wanatasanapan, M. Z. Abdullah, and P. Gunnasegaran, "Effect of TiO_2-Al_2O_3 nanoparticle mixing ratio on the thermal conductivity, rheological properties, and dynamic viscosity of water-based hybrid nanofluid," *J. Mater. Res. Technol.*, vol. 9, no. 6, pp. 13781–13792, Nov. 2020, doi: 10.1016/j.jmrt.2020.09.127.

[40] M. C. S. Reddy and V. V. Rao, "Experimental studies on thermal conductivity of blends of ethylene glycol-water-based TiO_2 nanofluids," *Int. Commun. Heat Mass Transf.*, vol. 46, pp. 31–36, Aug. 2013, doi: 10.1016/j.icheatmasstransfer.2013.05.009.

[41] M. Ullah, M. M. Hasan, R. Roslan, R. Jose, and I. I. Misnon, "Sustainable graphitic carbon derived from oil palm frond biomass for supercapacitor application: Effect of redox additive and artificial neural network-based modeling approach," *J. Electroanal. Chem.*, vol. 971, Oct. 2024, Art. no. 118570, doi: 10.1016/j.jelechem.2024.118570.

[42] T. Hai, K. H. Hama Aziz, J. Zhou, H. A. Dhahad, K. Sharma, S. F. Almojil, A. Ibrahim Almohana, A. F. Alali, T. I. Kh, S. Mehrez, and A. Abdelrahman, "Neural network-based optimization of hydrogen fuel production energy system with proton exchange electrolyzer supported nanomaterial," *Fuel*, vol. 332, Jan. 2023, Art. no. 125827, doi: 10.1016/j.fuel.2022.125827.

[43] L. F. Terrence, *Feedforward Neural Network Methodology*. Cham, Switzerland: Springer, 1999.

[44] C. Cortes and V. Vapnik, "Support-vector networks," *Mach. Learn.*, vol. 20, no. 3, pp. 273–297, 1995, doi: 10.1023/a:1022627411411.

[45] S. Salcedo-Sanz, J. L. Rojo-Álvarez, M. Martínez-Ramón, and G. Camps-Valls, "Support vector machines in engineering: An overview," *WIREs Data Mining Knowl. Discovery*, vol. 4, no. 3, pp. 234–267, May 2014, doi: 10.1002/widm.1125.

[46] X. Wei, L. Zhu, Y. Zeng, K. Xue, Y. Dai, J. Xu, G. Liu, F. Liu, W. Xue, D. Wu, and G. Wu, "Detection of prostate cancer using diffusion-relaxation correlation spectrum imaging with support vector machine model—A feasibility study," *Cancer Imag.*, vol. 22, no. 1, p. 77, Dec. 2022, doi: 10.1186/s40644-022-00516-9.

[47] P. Ebrahimi, A. Salamzadeh, M. Soleimani, S. M. Khansari, H. Zarea, and M. Fekete-Farkas, "Startups and consumer purchase behavior: Application of support vector machine algorithm," *Big Data Cognit. Comput.*, vol. 6, no. 2, p. 34, Mar. 2022, doi: 10.3390/bdcc6020034.

[48] H. Adun, I. Wole-Osho, E. C. Okonkwo, O. Bamisile, M. Dagbasi, and S. Abbasoglu, "A neural network-based predictive model for the thermal conductivity of hybrid nanofluids," *Int. Commun. Heat Mass Transf.*, vol. 119, Dec. 2020, Art. no. 104930, doi: 10.1016/j.icheatmasstransfer.2020.104930.

[49] P. S. Kojic, S. S. Popovic, M. S. Tokic, I. M. Šijacki, N. L. Lukić, D. Z. Jovicevic, and D. L. Petrovic, "Hydrodynamics of an external-loop airlift reactor with inserted membrane," *Brazilian J. Chem. Eng.*, vol. 34, no. 2, pp. 493–505, Apr. 2017, doi: 10.1590/0104-6632.20170342s20150399.

[50] K. J. Law, "Bayesian support vector regression," in *Proc. Int. Workshop Artif. Intell. Statist.*, 2001, pp. 239–244.

[51] I. O. Alade, M. A. A. Rahman, and T. A. Saleh, "An approach to predict the isobaric specific heat capacity of nitrides/ethylene glycol-based nanofluids using support vector regression," *J. Energy Storage*, vol. 29, Jun. 2020, Art. no. 101313, doi: 10.1016/j.est.2020.101313.

[52] I. O. Alade, M. A. A. Rahman, and T. A. Saleh, "Modeling and prediction of the specific heat capacity of Al_2O_3/water nanofluids using hybrid genetic algorithm/support vector regression model," *Nano-Struct. Nano-Objects*, vol. 17, pp. 103–111, Jun. 2019.

[53] J. A. K. Suykens and J. Vandewalle, "Recurrent least squares support vector machines," *IEEE Trans. Circuits Syst. I, Fundam. Theory Appl.*, vol. 47, no. 7, pp. 1109–1114, Jul. 2000, doi: 10.1109/81.855471.

[54] J. A. K. Suykens and J. Vandewalle, "Training multilayer perceptron classifiers based on a modified support vector method," *IEEE Trans. Neural Netw.*, vol. 10, no. 4, pp. 907–911, Jul. 1999, doi: 10.1109/72.774254.

[55] R. Henao, X. Yuan, and L. Carin, "Bayesian nonlinear support vector machines and discriminative factor modeling," in *Proc. Adv. Neural Inf. Process. Syst.*, 2014, p. 27.

[56] T. Law and J. Shawe-Taylor, "Practical Bayesian support vector regression for financial time series prediction and market condition change detection," *Quant. Finance*, vol. 17, no. 9, pp. 1403–1416, Sep. 2017, doi: 10.1080/14697688.2016.1267868.

[57] J. Wang, Y. Zhai, P. Yao, M. Ma, and H. Wang, "Established prediction models of thermal conductivity of hybrid nanofluids based on artificial neural network (ANN) models in waste heat system," *Int. Commun. Heat Mass Transf.*, vol. 110, Jan. 2020, Art. no. 104444, doi: 10.1016/j.icheatmasstransfer.2019.104444.

[58] M. Afrand, M. Hemmat Esfe, E. Abedini, and H. Teimouri, "Predicting the effects of magnesium oxide nanoparticles and temperature on the thermal conductivity of water using artificial neural network and experimental data," *Phys. E, Low-Dimensional Syst. Nanostruct.*, vol. 87, pp. 242–247, Mar. 2017, doi: 10.1016/j.physe.2016.10.020.

[59] E. Cengiz, M. Babagiray, F. Emre Aysal, and F. Aksoy, "Kinematic viscosity estimation of fuel oil with comparison of machine learning methods," *Fuel*, vol. 316, May 2022, Art. no. 123422, doi: 10.1016/j.fuel.2022.123422.

[60] J. D'Errico, "Surface fitting using gridfit," *MATLAB Cent. File Exch.*, vol. 643, pp. 1–24, May 2005.

[61] G. Maji, D. Mondal, N. Dey, N. C. Debnath, and S. Sen, "Stock prediction and mutual fund portfolio management using curve fitting techniques," *J. Ambient Intell. Humanized Comput.*, vol. 12, no. 10, pp. 9521–9534, Oct. 2021, doi: 10.1007/s12652-020-02693-6.

[62] S. Chakraborty and P. K. Panigrahi, "Stability of nanofluid: A review," *Appl. Thermal Eng.*, vol. 174, Jun. 2020, Art. no. 115259, doi: 10.1016/j.applthermaleng.2020.115259.

[63] A. Ghadimi, R. Saidur, and H. S. C. Metselaar, "A review of nanofluid stability properties and characterization in stationary conditions," *Int. J. Heat Mass Transf.*, vol. 54, nos. 17–18, pp. 4051–4068, Aug. 2011, doi: 10.1016/j.ijheatmasstransfer.2011.04.014.

[64] H. W. Xian, N. A. C. Sidik, and R. Saidur, "Impact of different surfactants and ultrasonication time on the stability and thermophysical properties of hybrid nanofluids," *Int. Commun. Heat Mass Transf.*, vol. 110, Jan. 2020, Art. no. 104389, doi: 10.1016/j.icheatmasstransfer.2019.104389.

[65] A. Albojamal and K. Vafai, "Analysis of particle deposition of nanofluid flow through porous media," *Int. J. Heat Mass Transf.*, vol. 161, Nov. 2020, Art. no. 120227, doi: 10.1016/j.ijheatmasstransfer.2020.120227.

[66] A. R. I. Ali and B. Salam, "A review on nanofluid: Preparation, stability, thermophysical properties, heat transfer characteristics and application," *Social Netw. Appl. Sci.*, vol. 2, no. 10, p. 1636, Oct. 2020, doi: 10.1007/s42452-020-03427-1.

[67] A. A. M. Redhwan, W. H. Azmi, M. Z. Sharif, and R. Mamat, "Development of nanorefrigerants for various types of refrigerant based: A comprehensive review on performance," *Int. Commun. Heat Mass Transf.*, vol. 76, pp. 285–293, Aug. 2016, doi: 10.1016/j.icheatmasstransfer.2016.06.007.

[68] J. Jacob, P. Preetha, and T. K. Sindhu, "Stability analysis and characterization of natural ester nanofluids for transformers," *IEEE Trans. Dielectr. Electr. Insul.*, vol. 27, no. 5, pp. 1715–1723, Oct. 2020, doi: 10.1109/TDEI.2020.008445.

[69] S. Sarbolookzadeh Harandi, A. Karimipour, M. Afrand, M. Akbari, and A. D'Orazio, "An experimental study on thermal conductivity of F-MWCNTs–Fe_3O_4 /EG hybrid nanofluid: Effects of temperature and concentration," *Int. Commun. Heat Mass Transf.*, vol. 76, pp. 171–177, Aug. 2016, doi: 10.1016/j.icheatmasstransfer.2016.05.029.

[70] J. Garg, B. Poudel, M. Chiesa, J. B. Gordon, J. J. Ma, J. B. Wang, Z. F. Ren, Y. T. Kang, H. Ohtani, J. Nanda, G. H. McKinley, and G. Chen, "Enhanced thermal conductivity and viscosity of copper nanoparticles in ethylene glycol nanofluid," *J. Appl. Phys.*, vol. 103, no. 7, Apr. 2008, Art. no. 074301, doi: 10.1063/1.2902483.

[71] H. Younes, M. Mao, S. M. Sohel Murshed, D. Lou, H. Hong, and G. P. Peterson, "Nanofluids: Key parameters to enhance thermal conductivity and its applications," *Appl. Thermal Eng.*, vol. 207, May 2022, Art. no. 118202, doi: 10.1016/j.applthermaleng.2022.118202.

[72] K. A. Hamid, W. H. Azmi, R. Mamat, and K. V. Sharma, "Experimental investigation on heat transfer performance of TiO_2 nanofluids in water–ethylene glycol mixture," *Int. Commun. Heat Mass Transf.*, vol. 73, pp. 16–24, Apr. 2016, doi: 10.1016/j.icheatmasstransfer.2016.02.009.

[73] M. R. Azizian, H. S. Aybar, and T. Okutucu, "Effect of nanoconvection due to Brownian motion on thermal conductivity of nanofluids," in *Proc. 7th IASM /WSEAS Int. Conf. Heat Transfer, Thermal Eng. Environ.*, 2009, pp. 53–56.

[74] D. K. Agarwal, A. Vaidyanathan, and S. Sunil Kumar, "Investigation on convective heat transfer behaviour of kerosene-Al_2O_3 nanofluid," *Appl. Thermal Eng.*, vol. 84, pp. 64–73, Jun. 2015, doi: 10.1016/j.applthermaleng.2015.03.054.

[75] M. Sheikholeslami, M. B. Gerdroodbary, R. Moradi, A. Shafee, and Z. Li, "Application of neural network for estimation of heat transfer treatment of Al_2O_3-H_2O nanofluid through a channel," *Comput. Methods Appl. Mech. Eng.*, vol. 344, pp. 1–12, Feb. 2019, doi: 10.1016/j.cma.2018.09.025.

[76] F. Sahin, O. Genc, M. Gökcek, and A. B. Çolak, "An experimental and new study on thermal conductivity and zeta potential of Fe_3O_4/water nanofluid: Machine learning modeling and proposing a new correlation," *Powder Technol.*, vol. 420, Apr. 2023, Art. no. 118388, doi: 10.1016/j.powtec.2023.118388.

[77] P. Sharma, K. Ramesh, R. Parameshwaran, and S. S. Deshmukh, "Thermal conductivity prediction of titania-water nanofluid: A case study using different machine learning algorithms," *Case Stud. Thermal Eng.*, vol. 30, Feb. 2022, Art. no. 101658, doi: 10.1016/j.csite.2021.101658.

[78] S. Rostami, R. Kalbasi, N. Sina, and A. S. Goldanlou, "Forecasting the thermal conductivity of a nanofluid using artificial neural networks," *J. Thermal Anal. Calorimetry*, vol. 145, no. 4, pp. 2095–2104, Aug. 2021, doi: 10.1007/s10973-020-10183-2.

[79] A. Alizadeh, K. J. Mohammed, G. F. Smaisim, S. K. Hadrawi, H. Zekri, H. T. Andani, N. Nasajpour-Esfahani, and D. Toghraie, "Evaluation of the effects of the presence of ZnO-TiO_2 (50%–50%) on the thermal conductivity of ethylene glycol base fluid and its estimation using artificial neural network for industrial and commercial applications," *J. Saudi Chem. Soc.*, vol. 27, no. 2, Mar. 2023, Art. no. 101613, doi: 10.1016/j.jscs.2023.101613.

[80] E. Onyiriuka, "Predictive modelling of thermal conductivity in single-material nanofluids: A novel approach," *Bull. Nat. Res. Centre*, vol. 47, no. 1, p. 140, Sep. 2023, doi: 10.1186/s42269-023-01115-9.

[81] M. A. Hassan, M. A. Hassan, D. Banerjee, and H. Hegab, "Evolutionary optimization of thermo-physical properties of MWCNT-Fe_3O_4/water hybrid nanofluid using least-squares support vector regression-based models," *Appl. Soft Comput.*, vol. 130, Nov. 2022, Art. no. 109644, doi: 10.1016/j.asoc.2022.109644.

[82] X. Yang, A. Boroomandpour, S. Wen, D. Toghraie, and F. Soltani, "Applying artificial neural networks (ANNs) for prediction of the thermal characteristics of water/ethylene glycol-based mono, binary and ternary nanofluids containing MWCNTs, titania, and zinc oxide," *Powder Technol.*, vol. 388, pp. 418–424, Aug. 2021, doi: 10.1016/j.powtec.2021.04.093.

[83] C. Lin, J. Zhou, Q. Lu, M. K. Khabaz, A. K. Andani, M. Al-Yasiri, and G. Pan, "Thermal conductivity prediction of WO_3-CuO-Ag (35:40:25)/water hybrid ternary nanofluid with artificial neural network and back-propagation algorithm," *Mater. Today Commun.*, vol. 36, Aug. 2023, Art. no. 106807, doi: 10.1016/j.mtcomm.2023.106807.

[84] N. Kishore P V R, S. Venkatachalapathy, P. Kalidoss, and P. Chaupal, "Experimental investigation with ANN modeling of thermal conductivity and viscosity of a ternary nanofluid at different mixing ratios and volume concentrations," *J. Mol. Liquids*, vol. 383, Aug. 2023, Art. no. 122006, doi: 10.1016/j.molliq.2023.122006.

[85] M. H. Esfe and D. Toghraie, "An optimal feed-forward artifcial neural network model and a new empirical correlation for prediction of the relative viscosity of Al_2O_3-engine oil nanofuid," *Sci. Rep.*, vol. 11, no. 1, 2021, Art. no. 17072.

[86] A. A. Melaibari, Y. Khetib, A. K. Alanazi, S. M. Sajadi, M. Sharifpur, and G. Cheraghian, "Applying artificial neural network and response surface method to forecast the rheological behavior of hybrid nano-antifreeze containing graphene oxide and copper oxide nanomaterials," *Sustainability*, vol. 13, no. 20, p. 11505, Oct. 2021, doi: 10.3390/su132011505.

[87] A. Asadi, I. M. Alarifi, H. M. Nguyen, and H. Moayedi, "Feasibility of least-square support vector machine in predicting the effects of shear rate on the rheological properties and pumping power of MWCNT–MgO/oil hybrid nanofluid based on experimental data," *J. Thermal Anal. Calorimetry*, vol. 143, no. 2, pp. 1439–1454, Jan. 2021, doi: 10.1007/s10973-020-09279-6.

MD. MUNIRUL HASAN received the B.S. degree in electrical and electronic engineering (EEE) from International Islamic University Chittagong (IIUC), and the M.S. degree in computer science from Universiti Malaysia Pahang Al-Sultan Abdullah, where he is currently pursuing the Ph.D. degree with the Faculty of Computing. His research interests include artificial intelligence, machine learning, deep learning, neural networks, and wireless communication.

MD. MUSTAFIZUR RAHMAN (Member, IEEE) received the B.Sc. and M.Sc. degrees in mechanical engineering from Bangladesh University of Engineering and Technology, and the Ph.D. degree from Universiti Kebangsaan Malaysia

He is currently a distinguished academic and a Researcher with the Faculty of Mechanical and Automotive Engineering Technology, Universiti Malaysia Pahang Al-Sultan Abdullah (UMPSA). His exemplary academic leadership is evidenced through his roles as the former Dean of Research and the Deputy Director of the Automotive Engineering Centre, UMPSA. He has established himself as a leading authority in engineering research and education. His academic journey includes significant positions with Khulna University of Engineering and Technology and leadership as the Department Head of the Shahjalal University of Science and Technology, demonstrating his progressive impact in engineering education. His commitment to advancing engineering education is further demonstrated through his successful mentorship of numerous Ph.D. and M.Sc. candidates, contributing significantly to developing the next generation of engineering professionals. His synthesis of academic excellence, research innovation, and leadership continues to advance the engineering field, particularly in sustainable technologies and advanced manufacturing processes, making him a pivotal figure in contemporary engineering education and research. His research interests include internal combustion engines, alternative fuels, heat transfer, nanoparticle coolants, applied and computational mechanics, advanced machining, and finite element analysis.

Prof. Rahman's professional standing is reinforced through fellowships in the Association of Computer, Electronics and Electrical Engineers and Indian Society of Mechanical Engineers, along with senior membership in American Society of Mechanical Engineers. As a Founder Member of Malaysian Society for Engineering and Technology, he continues to shape the engineering landscape in Malaysia and beyond. His influence in academic publishing is particularly noteworthy as the formal Editor-in-Chief of both the *International Journal of Automotive and Mechanical Engineering* and the *Journal of Mechanical Engineering and Sciences*.

MD. ARAFATUR RAHMAN (Senior Member, IEEE) received the Ph.D. degree in electronic and telecommunications engineering from the University of Naples Federico II, Naples, Italy, in 2013. He has around 15 years of research and teaching experience in the domain of computer science and communications engineering. He was an Associate Professor with the Faculty of Computing, Universiti Malaysia Pahang (UMP). He was a Postdoctoral Research Fellow with the University of Naples Federico II, in 2014, and a Visiting Researcher with the Sapienza University of Rome, in 2016. He was a fellow with the IBM Center of Excellence and the Earth Resources and Sustainability Center, Malaysia. He is currently a Reader of cyber security with the School of Engineering, Computing and Mathematical Sciences, University of Wolverhampton, U.K. He has co-authored around 150 prestigious IEEE and Elsevier journals, such as IEEE TRANSACTIONS ON INDUSTRIAL INFORMATICS, IEEE TRANSACTIONS ON INTELLIGENT TRANSPORTATION SYSTEMS, IEEE TRANSACTIONS ON GREEN COMMUNICATIONS AND NETWORKING, IEEE TRANSACTIONS ON SERVICES COMPUTING, *IEEE Communications Magazine*, *Journal of Network and Computer Applications* (Elsevier), and *Future Generation Computer Systems* (Elsevier), and conference publications, such as IEEE GLOBECOM and IEEE DASC). He has developed an excellent track record of academic leadership and management and execution of international ICT projects that are supported by agencies in U.K., Italy, EU, and Malaysia. His research interests include cyber security in particular focus on the Internet of Things (IoT), wireless communication networks, cognitive radio networks, 5G, vehicular communication, cyber physical systems, big data, cloud-fog-edge computing, and machine learning dependent applications. He received a number of prestigious international research awards, notably the Best Paper Award at ICNS-15 (Italy), the IC0902 Grant (France), Italian Government Ph.D. Research Scholarship, the IIUM Best Masters Student Award, and the Best Supervisor Award at UMP, and the awards in international exhibitions, including the Euro Business-HALLER Poland Special Award, the MTE 2022, the Best Innovation Award, the MTE 2020, Malaysia, the Diamond and Gold in BiS-17 U.K., the Best of the Best Innovation Award, the Most Commercial IT Innovation Award, Malaysia, and the Gold and Silver medals in iENA-17 Germany. His name was enlisted inside the world top two university under the category of ''Citation Impact in Single Calendar Year, in 2019, 2020, and 2021.'' He was awarded the Higher Education Academy (HEA) Fellowship from U.K. He was endorsed by the Royal Academy of Engineering, U.K., as a Global Talent under the category of ''Exceptional Talent,'' in 2022. He served as the General Chair, the Organizing Committee Chair, the Publicity Chair, the Session Chair, the Program Committee Chair, and a member of the Technical Program Committee (TPC) for numerous leading conferences worldwide (e.g., IEEE GLOBECOM, IEEE DASC, IEEE iSCI, and IEEE ETCCE) and journals. He served as the Specialty Chief Editor for *IoT Theory and Fundamental Research* (specialty section of *Frontiers in the Internet of Things*); an Advisory Board Member and an Editorial Board Member for *Computer Systems Science and Engineering*, Tech Science Press, and *Computers* (MDPI), respectively; the Lead Guest Editor for IEEE ACCESS and *Computers*; and an Associate Editor for IEEE ACCESS and *Patron*.

SURAYA ABU BAKAR received the B.S. degree in computer science from Universiti Malaya, and the M.S. degree in computer science from Universiti Malaysia Terengganu, Malaysia. She is currently a Senior Lecturer with Universiti Malaysia Pahang Al-Sultan Abdullah, Malaysia. Her research interests include image processing, embedded systems, artificial intelligence, computer vision, and the Internet of Things (IoT).

MOHAMMAD SAIFUL ISLAM received the B.S. degree in electrical and electronic engineering from the International University of Business Agriculture and Technology, in 2018, and the M.S. degree in electrical and electronics engineering from Islamic University, Kushtia, in 2019. He is currently pursuing the Master of Science degree in information technology with the St. Francis College, New York.

TAREK KHALIFA received the B.Sc. degree in electrical and computer engineering from the University of Tripoli, Libya, in 2000, and the M.Sc. and Ph.D. degrees from the University of Waterloo, Canada, in 2007 and 2013, respectively. He is currently an Assistant Professor with American University of the Middle East, Kuwait. His research interests include network security, sensors and power grid networks, and machine learning in the medical field.